



1 MICS-Asia III: Multi-model comparison of reactive Nitrogen deposition  
2 over China

3 Baozhu Ge<sup>1,2</sup>, Syuichi Itahashi<sup>3</sup>, Keiichi Sato<sup>4</sup>, Danhui Xu<sup>1,5</sup>, Junhua Wang<sup>1,5</sup>, Fan  
4 Fan<sup>6</sup>, Qixin Tan<sup>1,5</sup>, Joshua S. Fu<sup>7</sup>, Xuemei Wang<sup>8</sup>, Kazuyo Yamaji<sup>9</sup>, Tatsuya  
5 Nagashima<sup>10</sup>, Jie Li<sup>1,2,5</sup>, Mizuo Kajino<sup>11,12</sup>, Hong Liao<sup>13</sup>, Meigen Zhang<sup>1,2,5</sup>, Zhe  
6 Wang<sup>1,2,14</sup>, Meng Li<sup>15</sup>, Jung-Hun Woo<sup>16</sup>, Jun-ichi Kurokawa<sup>17</sup>, Yuepen Pan<sup>1</sup>, Qizhong  
7 Wu<sup>18</sup>, Xuejun Liu<sup>19</sup> and Zifa Wang<sup>1,2,5</sup>

8  
9 <sup>1</sup> State Key Laboratory of Atmospheric Boundary Layer Physics and Atmospheric Chemistry  
10 (LAPC), Institute of Atmospheric Physics (IAP), Chinese Academy of Sciences (CAS), Beijing  
11 100029, China

12 <sup>2</sup> Center for Excellence in Urban Atmospheric Environment, Institute of Urban Environment,  
13 Chinese Academy of Sciences (CAS), Xiamen 361021, China

14 <sup>3</sup> Environmental Science Research Laboratory, Central Research Institute of Electric Power  
15 Industry (CRIEPI), Abiko, Chiba 270-1194, Japan

16 <sup>4</sup> Asia Center for Air Pollution Research (ACAP), 1182 Sowa, Nishi-ku, Niigata, Niigata 950-2144,  
17 Japan

18 <sup>5</sup> Collage of Earth Science, University of Chinese Academy of Sciences, Beijing 100049, China

19 <sup>6</sup> Nanjing Intelligent Environmental Sci-Tech Co., Ltd., Nanjing, 211800, China

20 <sup>7</sup> Department of Civil and Environmental Engineering, University of Tennessee, Knoxville, TN  
21 37996, USA

22 <sup>8</sup> Institute for Environmental and Climate Research, Jinan University, Guangzhou 510632, China

23 <sup>9</sup> Graduate School of Maritime Sciences, Kobe University, Kobe, Hyogo 658-0022, Japan

24 <sup>10</sup> National Institute for Environmental Studies (NIES), Tsukuba, Ibaraki 305-8506, Japan

25 <sup>11</sup> Meteorological Research Institute (MRI), Tsukuba, Ibaraki 305-8506, Japan

26 <sup>12</sup> Faculty of Life and Environmental Sciences, University of Tsukuba, Tsukuba, Ibaraki 305-8506,  
27 Japan

28 <sup>13</sup> School of Environmental Science and Engineering, Nanjing University of Information Science  
29 & Technology, Nanjing 210044, China

30 <sup>14</sup> Research Institute for Applied Mechanics (RIAM), Kyushu Univeristy, Kasuga, Fukuoka 816-  
31 8580, Japan

32 <sup>15</sup> Ministry of Education Key Laboratory for Earth System Modeling, Department of Earth System  
33 Science, Tsinghua University, Beijing 100084, China

34 <sup>16</sup> Division of Interdisciplinary Studies, Department of Advance Technology Fusion, Konkuk  
35 University, Seoul, 303-804, Korea

36 <sup>17</sup> Asia Center for Air Pollution Research (ACAP), 1182 Sowa, Nishi-ku, Niigata, Niigata  
37 950-2144, Japan

38 <sup>18</sup> College of Global Change and Earth System Science, Beijing Normal University, Beijing  
39 100875, China

40 <sup>19</sup> College of Resources & Environmental Sciences, China Agricultural University, Beijing 100193,  
41 China.

42

43 *Correspondence to:* Baozhu Ge (gebz@mail.iap.ac.cn)



44 **Abstract:** Atmospheric nitrogen deposition in China has attracted huge public  
45 attention in recently years due to the increasing anthropogenic emission of reactive  
46 nitrogen ( $N_r$ ) and its impacts on the terrestrial and aquatic ecosystems. However,  
47 limited long-term and multi-site measurements have restrained the understanding on  
48 the mechanism of the  $N_r$  deposition as well as the chemical transport model (CTM)  
49 improvement. In this study, the performance of the simulated wet and dry deposition  
50 for different  $N_r$  species, i.e., particulate  $NO_3^-$  and  $NH_4^+$ , gaseous  $NO_x$ ,  $HNO_3$  and  $NH_3$ ,  
51 have been conducted using the framework of Model Inter-Comparison Study for Asia  
52 (MICS-Asia) phase III. Nine Models, including 5 WRF-CAMQ models, 2  
53 self-developed regional models, a global model and a RAMS-CMAQ model, have  
54 been selected for the comparison. For wet depositions, observation data from 83  
55 measurement sites of EANET, CREAN, CAUDN, NADMN and DEE of China have  
56 been collected and normalized to compare with model results. In general, most  
57 models showed the consistent spatial and temporal variation of both oxidized N ( $N_{ox}$ )  
58 and reduced N ( $N_{rd}$ ) wet depositions in China with the NME around at 50%, which is  
59 lower than the value of 70% based on EANET observation over Asia. Both the ratio  
60 of wet or dry deposition to the total inorganic N deposition (TIN) and the ratios of  
61 TIN to their emissions have shown the consistent results with the NNDMN  
62 estimations. The performance of ensemble results (ENM) was further assessed with  
63 the measurement from satellite. In different regions of China, the results showed that  
64 the simulated  $N_{ox}$  wet deposition was overestimated in North East China (NE) but  
65 underestimated in south of China (SE+SW), while the  $N_{rd}$  wet deposition was  
66 underpredicted in all regions by all models. The deposition of  $N_{ox}$  have large  
67 uncertainties than the  $N_{rd}$  especially in North China (NC), indicating chemical  
68 reaction process is one of the most importance factors that affecting the model  
69 performance. Compared to Critical load (CL) value, the  $N_r$  deposition in NC, SE and  
70 SW reached or exceeded the reported CL value and exerted serious ecological impacts.  
71 The control of  $N_{rd}$  in NC and SW and  $N_{ox}$  in SE would be effective to mitigate the  
72 TIN deposition in these regions. More interestingly, the  $N_r$  deposition in Tibet plateau  
73 with the high ratio of TIN/emission ( $\sim 3.0$ ), indicating a significant import from  
74 outside should be focused in the future due to its climatical influence to the sensitive  
75 ecosystem in whole China.

76

77 **Keywords:** Nitrogen deposition, multi-model comparison, China, reduced nitrogen,  
78 oxidized nitrogen



## 79 **1 Introduction**

80 Atmospheric Nitrogen (N) deposition is defined that N related gases and particles are  
81 deposited via precipitation (wet deposition) and not via precipitation (dry deposition)  
82 (Clark and Kremer, 2005). These depositions to the Earth's surface, are either close to  
83 the sources or in remote regions (e.g. chemical transformation and long-range  
84 transport of oxidized and reduced N,  $N_{ox}$  and  $N_{rd}$  hereafter), where is located far from  
85 human activities and labeled as the N-limited areas (Phoenix et al., 2006; Holtgrieve et  
86 al., 2011). Evidences show that the effects of reactive N ( $N_r=N_{ox}+N_{rd}$ ) deposition to  
87 environment are numerous, including decreased biological diversity, increased soil  
88 acidification, and lake eutrophication (Clark and Tilman, 2008; Janssens et al.,  
89 2010; Holtgrieve et al., 2011; Phoenix et al., 2006; Galloway et al., 2004). Different  
90 human activities disturb the natural N cycle in serious manners (Galloway et al.,  
91 2004), for example using artificial fertilizer to increase crop production (Erismann et  
92 al., 2008) or relying too much fossil fuel for industrial production. The  $N_r$  production  
93 increased from approximately  $15 \text{ Tg N yr}^{-1}$  in 1860 to  $187 \text{ Tg N yr}^{-1}$  in 2005 and more  
94 than 50% of them have been reported to deposit onto the ground (Nicolas and  
95 Galloway, 2008). In the past two decades, high rates of  $N_r$  deposition were widely  
96 documented in the developed countries such as America (Fenn et al., 1998) and  
97 Europe (Dise and Wright, 1995). Great efforts have been made to fight against these  
98 negative effects in USA to decrease  $NO_x$ , and the  $N_{ox}$  deposition was decreased  
99 dramatically in recent years (Li et al., 2016). However, the growing human demand  
100 for food and energy at a global scale resulted in an increasing emission of  $N_r$  into  
101 environment (Galloway et al., 2008), particularly in large developing countries like  
102 China and India (Chen et al., 2019a; Liu et al., 2013).

103 A nationwide estimation of long-term N deposition in China based on the bulk  
104 measurements as well as summarizing from reported references in 270 sites by Liu et  
105 al. (2013) shown an increasing rate of  $0.41 \text{ kg N ha}^{-1}$  per year from 1980 to 2010.  
106 Different from the increasing importance of  $N_{rd}$  deposition due to apparently  
107 decreasing of  $N_{ox}$  that benefit from the air quality control in USA in past decades (Li  
108 et al., 2016), the ratio of  $N_{rd}/N_{ox}$  recorded from bulk/wet deposition decreased from 5  
109 in 1980 to 2 in 2010 indicating the more and more important role of  $N_{ox}$  in China (Liu  
110 et al., 2013). The ratio in highly developed regions such as North China Plain was  
111 even lower than 1 in recent years (Pan et al., 2012). However, very limited long-term  
112 observations in China challenge our capacity to understand and control the increase of  
113  $N_r$  deposition. The published long-term N deposition monitoring network, which  
114 includes the Acid Deposition Monitoring Network in East Asia (EANET,  
115 <http://www.eanet.asia/index.html>), the National wide Nitrogen Deposition Monitoring  
116 Network (NNDMN) established since 2010 by China Agriculture University (CAU)  
117 (Xu et al., 2015), and the Chinese Ecosystem Research Network (CERN) in North  
118 China Plain established by Chinese Academy of Science (Pan et al., 2012), the Acid  
119 Rain Monitoring Network run by the China Meteorological Administration  
120 (CMA-ARMN) (Tang et al., 2007; Tang et al., 2010; Ge et al., 2011), and the National  
121 Acid Deposition Monitoring Network (NADMN) (Li et al., 2019b), have been  
122 identified with many shortcomings, e.g. the scattered monitoring sites as well as the



123 uncompleted recorded data, due to high cost of the measurement against the unstable  
124 financial support. Chemical Transport Model (CTM) simulation is another option to  
125 offset these drawbacks and also to quantify long-range transport of deposition in a  
126 global or regional map (Seinfeld and Pandis, 2006). It is important to know the  
127 accuracy of the CTM before it is employed to investigate the spatial and temporal  
128 variation of the depositions. Hayami et al. (2008) and Mann et al. (2014) referred that  
129 different parameterization set in CTMs may result in large variations, and the  
130 multi-model ensemble mean (ENM) shows better performance than most single one  
131 (Carmichael et al., 2002; Hayami et al., 2008; Holloway et al., 2008; Wang et al., 2008).  
132 Besides, to better localize applications of CTM, the comprehensive evaluations of the  
133 strengths and weaknesses of current CTMs for simulating the acid deposition as well  
134 as their precursors in a unified framework, with certain regulated rules and same  
135 inputs to models, should be more critical and effective.

136 Model Inter-Comparison Study for Asia (MICS-Asia) gives an opportunity to  
137 investigate the CTMs application with different models in Asia. MICS-Asia was  
138 initiated in 1998 with the target of long-range transport and deposition in  $\text{SO}_4^{2-}$  in the  
139 first stage (MICS-Asia phase I) (Carmichael et al., 2002) and sulfur, nitrogen and  
140 ozone in the second stage (MICS-Asia phase II) (Carmichael et al., 2008). The  
141 findings concluded and the methodologies developed in the previous inter-comparison  
142 studies undoubtedly contributed to common understandings of the performance and  
143 uncertainties of CTMs applications in East Asian (Hayami et al., 2008; Carmichael et  
144 al., 2008; Han et al., 2008; Wang et al., 2008). The comprehensive multi-model  
145 inter-comparison study on the acid deposition in China is becoming urgent issue as  
146 the high emissions in China causing acid deposition in neighboring countries (Lin et  
147 al., 2008; Kajino et al., 2011; 2013; Itahashi et al., 2018). In this study, one year  
148 simulated  $\text{N}_r$  depositions, i.e.  $\text{N}_{\text{ox}}$  and  $\text{N}_{\text{rd}}$  in both wet and dry deposited ways to the  
149 surface ground, using the framework of MICS-Asia III (MICS-Asia phase III), have  
150 been compared with each other and validated by the observed wet deposition from  
151 EANET, NNDMN, CREN and the Department of ecological environment (DEE,  
152 former named as Environmental Protect Administration, EPA) over the whole China.  
153 The rationale of the performance of the ENM results were also discussed by  
154 comparing with the Vertical Column Density (VCD) from satellite and the emission  
155 inventories. Finally, the uncertainties of the pathways to  $\text{N}_r$  depositions as well as its  
156 ecological impacts have been quantified. The results from this study will not only  
157 provide important reference for establishing a suitable N deposition model, the  
158 localized application of CTMs in China will also be tested.

## 159 **2 Framework of intercomparison in MICS-Asia III**

### 160 **2.1 Description of the participant models**

161 In the phase III of MICS-Asia, a total of 14 chemical transport models (CTM,  
162 M1-M14) participated in the topic of comparison and evaluation of current  
163 multi-scale air quality models (Named as topic 1 in MICS-Asia III). The same number  
164 index has been used in the deposition comparison part defined in aerosol and ozone  
165 comparison reported by Chen et al. (2019b) and Li et al. (2019a). However, the fully  
166 coupled online Weather Research and Forecasting model with chemistry



167 (WRF-Chem), which has been indexed as M7-M10, was not included in the  
168 deposition comparison part in the overview of model inter-comparison and evaluation  
169 for acid deposition in Asia (Itahashi et al., 2019). Briefly, Weather Research and  
170 Forecasting model coupled with Community Multi-scale Air Quality (WRF-CMAQ)  
171 has been numbered as M1-M6, with different version of v5.0.2 for M1 and M2, v5.0.1  
172 for M3 and v4.7.1 for M4-M6. M11 and M12 were the independent models developed  
173 by Japan and China, named as NHM-Chem (Kajino et al., 2019) and the nested air  
174 quality prediction model system (NAQPMS), respectively. A global three-dimensional  
175 chemical transport model (GEOS-Chem v9.1.3), numbered as M13, was also used as  
176 the long-range transport and future change prediction in MICS-Asia III. The last  
177 number of M14 was represented as the Regional Atmospheric Modeling System  
178 coupled with CMAQ (RAMS-CMAQ). It should be noted that the last two models,  
179 i.e., M13 and M14, were not driving by the “standard” meteorological fields from  
180 WRF v3.4.1 model. Basic information about the configuration of each model was  
181 summarized in Table 1. More detailed description could also be found in previous  
182 studies (Itahashi et al., 2019; Chen et al., 2019b; Li et al., 2019a).

## 183 **2.2 Model inputs and simulation domain**

184 As that mentioned by Chen et al. (2019b), same (“standard”) meteorological fields,  
185 emission inventories and boundary conditions have been prepared for the CTMs  
186 inter-comparison in MICS-Asia III to reduce the uncertainties from model inputs.  
187 However, some models such as M13 and M14 were imported “non-standard” inputs  
188 due to their specific characteristics. The “standard” meteorological inputs were  
189 simulated by WRF v3.4.1 with the initial and lateral boundary conditions from the  
190 National Centers for Environmental Prediction (NCEP) Final Analysis (FNL) data.  
191 Four dimensional data assimilation (FDDA) nudgings have been adopted every 6  
192 hours to improve the accuracy of the meteorological parameters simulation. The  
193 assimilated meteorological fields from the Goddard Earth Observing System 5  
194 (GEOS5) of the US 25 National Aeronautics and Space Administration (NASA)  
195 (<https://gmao.gsfc.nasa.gov>) were used to drive M13. The M14 model was driven by  
196 RAMS with the same FNL data for nudging as the “standard” WRF simulation, which  
197 is developed by Pielke et al. (1992). For the emission inputs, all the participant model  
198 were using the same emission inventory, which included the MIX anthropogenic  
199 emissions over Asia developed for MICS-Asia Phase III (Li et al., 2017), the biogenic  
200 emissions calculated by the Model of Emissions of Gases and Aerosols from Nature  
201 (MEGAN) version 2.04 (Guenther et al., 2006), and the biomass burning emissions  
202 from Global Fire Emission Database (GFED) version 3 (van der Werf et al., 2010).  
203 Besides, the SO<sub>2</sub> emissions from volcano were collected from AEROCOM program  
204 (<https://aerocom.met.no/> DATA/download/emissions/AEROCOM\_HC/volc, last ac-  
205 cess: 11 September 2019, Diehl et al., 2012; Stuefer et al., 2013). MICS-Asia Phase  
206 III provided two sets of lateral boundary conditions derived from GEOS-Chem (Bey  
207 et al., 2001) and CHASER (Sudo et al., 2002), respectively. The boundary conditions  
208 from GEOS-Chem were run with 2.5°×2° resolution and 47 vertical layers, while  
209 those from CHASER were run with 2.8°×2.8° and 32 vertical layers. M4, M5, M6,  
210 M11 and M12 used the output from CHASER as the boundary conditions, and M1,



211 M13 and M14 were from GEOS-Chem. Only M2 used the default boundary condition  
212 field provided in CMAQ.

213 The “standard” simulation domain covers the region of East Asia (15.4°S-58.3°N,  
214 48.5°E-160.2°E) with 180×170 grids at 45 km horizontal resolution. M1-M6, M11 and  
215 M12 followed “standard” simulation domain, while M13 and M14 employed different  
216 modeling domains with 0.5°latitude × 0.667°longitude and 64 × 64 km, respectively.  
217 In this study, the analyzed region was only focused in China and all participant  
218 models covered it. Therefore, simulated reactive N depositions in each model can be  
219 analyzed and compared to show the performance of the participant models. All  
220 models output of N depositions have been classified as oxidized N ( $N_{ox} = gHNO_3 +$   
221  $gNO_x + pNO_3^-$ , including gaseous nitrate acid,  $NO_x$  and particulate nitrate) and  
222 reduced N ( $N_{rd} = gNH_3 + pNH_4^+$ , including gaseous ammonia and particulate  
223 ammonium) for comparison.

### 224 2.3 Observation data

225 China has large area with almost 5,500 km from south to north (3.5°S-53.3°N) and  
226 5,200 km from west to east (75.5°E-135°E), which go through the coastal to inland and  
227 through tropical to Frigid Zone. Only 8 sites located in Guangdong, Fujian, Sichuan  
228 and Shanxi in EANET were not sufficient to show the real performance of CTMs in  
229 China. Besides the 8 EANET sites, 83 sites in total with daily or weekly and even  
230 yearly routine recorded data from the CERN (Pan et al., 2012), NNDMN (Xu et al.,  
231 2015;Liu et al., 2013) and DEE of Guangdong, Liaoning and Xinjiang province as  
232 well as Shanghai have been employed in this study to compare the simulated wet  
233 deposition in MICS-Asia III in China. Figure 1 displayed the location of 83  
234 measurement sites as well as the divided regions of the whole China. There were 50  
235 urban sites and 33 rural sites. More detailed information of each measurement site  
236 could also be found in Table S1 in the supplementary documents.

237 The daily wet deposition was measured by wet-only sampler to collect precipitation  
238 samples during the rainfall event in EANET. Analysis methods for  $NO_3^-$  and  $NH_4^+$   
239 were based on ion chromatography and checked by ion balance and conductivity  
240 agreement. Detailed description could be found on manual (EANET, 2010). Daily  
241 rainwater samples at 10 sites located in North China Plain were collected using a  
242 custom wet-dry automatic collector (APS-2B, Xianglan Scientific Instruments Co.,  
243 Ltd., Changsha, China) in CREN. Inorganic N, including  $NO_3^-$  and  $NH_4^+$ , in the  
244 precipitation samples was determined using an ion chromatography system (Model  
245 ICS- 90, Dionex Corporation, Sunnyvale, CA, USA) and the standard laboratory  
246 procedure of LAPC (Wang et al., 2012). The detection limit (DL) of N for this  
247 instrument was  $5 \mu g l^{-1}$ . Detailed description could be found in the research of Pan et  
248 al. (2012). The wet/bulk  $NO_3^-$  and  $NH_4^+$  deposition data from 25 sites of China  
249 Agricultural University Deposition Network (CAUDN), which was renamed as  
250 NNDMN in China since 2010, have been collected and reanalyzed as yearly data (Xu  
251 et al., 2015;Liu et al., 2013). At all monitoring sites precipitation samples were  
252 collected using precipitation gauges (SDM6, Tianjin Weather Equipment Inc., China)  
253 located beside the DELTA systems (ca. 2m, DENuder for Long-Term Atmospheric  
254 sampling). After collecting, the samples have been analyzed in CAU’s laboratory



255 based on the standard laboratory procedure of CAU (Xu et al., 2015). Routine  $\text{NO}_3^-$   
256 and  $\text{NH}_4^+$  wet depositions collected in each rainfall event at 40 sites have been  
257 provided by the DEE of Guangdong, Liaoning and Xinjiang province as well as  
258 Shanghai city. The analyzed procedure was followed as the laboratory procedure of  
259 China National Environmental Monitoring Centre (CNEMC).

260 All data from daily or rainfall event collecting samples at each type of  
261 measurement sites has been summarized and normalized as monthly wet deposition  
262 data to compare with the monthly simulation in MICS-Asia III in this study, except  
263 the yearly data provided by NNDMN. VCD of  $\text{NO}_2$  from SCIAMACHY  
264 (<http://www.temis.nl/airpollution/no2col>) and  $\text{NH}_3$  from IASI  
265 ([http://ether.ipsl.jussieu.fr/ether/pubipsl/iasial2/iasi\\_nh3](http://ether.ipsl.jussieu.fr/ether/pubipsl/iasial2/iasi_nh3)) have also been used to  
266 compare with the total deposition as well as the emissions.

### 267 **3 Results**

#### 268 **3.1 Validation of wet deposition**

##### 269 **3.1.1 Yearly comparison and monthly variation of oxidized N**

270 Yearly simulated wet deposition of  $\text{N}_{\text{ox}}$  has been evaluated by observed nitrate wet  
271 deposition in 83 sites over China. Table 2 listed the statistical parameters of simulated  
272 wet deposition of  $\text{N}_{\text{ox}}$  compared with the observed data in rural and urban sites of  
273 China. In all sites, M1, M5 and M11 overestimated the yearly wet deposition of  $\text{N}_{\text{ox}}$   
274 with Normalized Mean Bias (NMB) of +30.3%, +55.4% and +67.2%, respectively.  
275 M6, M12 and M13 simulated almost comparable results with NMB of -6.8%, +0.6%  
276 and +0.1%, respectively. M2, M4 and M14 underestimated the yearly wet deposition  
277 of  $\text{N}_{\text{ox}}$  with NMB of -38.7%, -10.7% and -47.4%, respectively. The NME was almost  
278 around at 50% with highest 82.2% in M11, which is lower than EANET observation  
279 over Asia with the value at 70% by Itahashi et al. (2019). However, the correlation  
280 coefficients R was around 0.2~0.3 (n=83) which is lower than EANET data (0.3~0.4,  
281 n=54) (Itahashi et al., 2019). In order to eliminate influences from rainfall  
282 uncertainties (R=0.82), the volume weighted mean (VWM) concentration of  $\text{N}_{\text{ox}}$  in  
283 precipitation has also been evaluated. In contrast to the low R value of yearly wet  
284 deposition of  $\text{N}_{\text{ox}}$ , the correlation R increased to almost 0.5 for the VWM  
285 concentrations. Approximately 50% of model results were corresponded within the  
286 percentages within a factor of 2 (FAC2). M1 and M13 performed better agreement  
287 with 60% and 59% within FAC2, while M2 and M14 showed only 36% and 45%  
288 agreement within FAC2. All of ground surface measurement sites have been divided  
289 into 49 urban sites and 34 rural sites according to their location. Overall, all the  
290 models showed better performance with the R in 0.2~0.4 and FAC2 in 50%~60% in  
291 urban sites than that of R in 0.05~0.3 and FAC2 in 40%~50% in rural sites. This  
292 difference may not due to the uncertainties in rainfall simulation, as the simulated  
293 VWM concentration of  $\text{N}_{\text{ox}}$  in precipitation may eliminate the rainfall uncertainties,  
294 and also shows better agreement in urban than that in rural sites (Table 2).

295 Figure 2 showed the percentile box plot the yearly wet deposition of  $\text{N}_{\text{ox}}$  simulated  
296 by 9 participant models in five regions of China (i.e., North China (NC), Northeastern  
297 China (NE), southeastern China (SE), northwestern China (NW), southwestern China  
298 and Tibet Plateau (SW+TP)). Site by site validation of both the yearly wet deposition



299 and VWM concentration of  $N_{ox}$  simulated by each model were also displayed in  
300 Figure S1. The model results showed large intra-region or inter-region uncertainties,  
301 especially in NC, NE and SE. The highest wet deposition of  $N_{ox}$  simulated by M11  
302 was almost 3~4 times of the lowest result simulated by M14 in the above regions  
303 (Figure 2). Specifically, two models simulated 30-50% higher of  $N_{ox}$  wet deposition,  
304 while four models were 20~40% lower compared to the averaged observations in NC  
305 with the averaged value  $6.5 \text{ kg N ha}^{-1} \text{ a}^{-1}$ . For the wet deposition of  $N_{ox}$  in SE and  
306 SW+TP, most of the participant models were more than 50% underestimated with the  
307 largest underestimation of 75% from M14, even though the precipitation in this region  
308 was overestimated. Besides, the divergence of observed  $N_{ox}$  wet deposition between  
309 different sites in NC, SE and SW, which was shown as the length of the red box in  
310 Figure 2a, 2d and 2e, was significantly larger than the multi-models results. The  
311 scattered distribution of the measurement sites in these regions was responsible for the  
312 large divergence in observations. However, most of the participant models failed to  
313 capture the large difference, indicating that the coarse grid in MICS-Asia III (45 km)  
314 was not suitable for the performance of detailed characterization at a local scale. A  
315 global assessment of the ensemble simulated wet depositions in the Task Force on  
316 Hemispheric Transport of Atmospheric Pollutants (TF HTAP) by Vet et al. (2014) also  
317 indicated the underprediction of the models in a number of sites in north America,  
318 Europe, Central Africa and part of East Asia. The underprediction in Europe was  
319 found due to the large underpredictions of precipitation depth, while the reason for  
320 East Asia is still unknown. However, most of the models overestimated the wet  
321 deposition of  $N_{ox}$  in NE. Several models including M1, M5 and M11 simulated more  
322 than  $10 \text{ kg N ha}^{-1} \text{ a}^{-1}$   $N_{ox}$  wet deposition, almost double higher than the observed value  
323 of  $5 \text{ kg N ha}^{-1} \text{ a}^{-1}$ . Both the multi-models and the observations showed very low  
324 values of 3-4  $\text{kg N ha}^{-1} \text{ a}^{-1}$   $N_{ox}$  wet deposition in NW, where the precipitation depth  
325 was very low compared to the other regions of China (Figure S1).

326 Further evaluations in temporal variations both in urban and rural sites of NC and  
327 NE have been displayed in Figure 3. Generally, all of the models and observations  
328 performed high level of depositions in spring and summer and low value in winter in  
329 the two regions. High depositions were due to large precipitation depth in rainy  
330 season. However, this was not always true in some urban sites. For example, higher  
331 depositions of  $N_{ox}$  were observed in May and June with lower rainfall volume than in  
332 July and August with higher rainfall in the urban sites of NC. Similar cases were  
333 found at urban sites in NE. Previous studies confirmed there is a decreasing trend in  
334 the variations of chemical components in precipitation as the rainfall evolution  
335 (Aikawa and Hiraki, 2009; Aikawa et al., 2014; Xu et al., 2017). If the rainfall lasted  
336 long enough, or rainfall volume was large enough, the concentrations of chemical  
337 components in precipitation remained at low levels and were attributed to the effects  
338 of the in-cloud scavenging process. That is, the large rainfall in an event may not  
339 cause the high level of monthly wet depositions due to the low level of in-cloud  
340 deposition compared to the wet deposited by several different precipitation events,  
341 especially in polluted regions in urban sites. Unfortunately, only monthly data of wet  
342 deposition as well as precipitation have been compared in this MICS-Asia III.





343 Detailed comparison with the rainfall event should be considered in the future.

### 344 **3.1.2 Yearly comparison and monthly variation of reduced N**

345 Simulated wet deposition of  $N_{rd}$  in MICS-Asia III has been evaluated using the  
346 multi-source of observations from the same sites as referred in  $N_{ox}$ . It is shown in  
347 Table 3 that all of the models underestimated the  $N_{rd}$  wet depositions with the  
348 negative NMB both in urban and rural sites. Although little difference between rural  
349 and urban sites was found in M11 and M14, a better performance in rural area was  
350 manifested from the lower NMB and higher FAC2 in rural sites than the urban sites in  
351 most of models (-13.6%~-23.2% vs -37.3%~-45.6% for NMB and 55.9-70.6% vs  
352 42.9-55.1% for FAC2, except M11 and M14). The underestimation of the simulated  
353  $N_{rd}$  wet depositions was also found in the VWM concentration of  $N_{rd}$  in precipitation  
354 with similar NMB and FAC2. However, compared with the wet deposition, the  
355 correlation between the simulated and observed  $N_{rd}$  VWM concentration in  
356 precipitation was significant with the R increased from ~0.3 to ~0.8, which was  
357 similar with that shown in  $N_{ox}$ . This indicated the simulated VWM concentration of  
358  $N_{rd}$  in precipitation by MICS-Asia III has better performance in spatial variation than  
359 the simulation of  $N_{rd}$  wet deposition over China.

360 Specifically, the performance of  $N_{rd}$  wet deposition prediction in MICS-Asia III has  
361 also been validated in five regions through the percentile box plot in Figure 4. Site by  
362 site validation of both the yearly wet deposition and VWM concentration of  $N_{rd}$   
363 simulated by each model were also displayed in Figure S2. Different from that found  
364 in  $N_{ox}$ , almost similar behavior prediction has been found in same models, i.e.,  
365 CMAQ models in M1~M6 but except M12 which was driven by different  
366 meteorological model. Other regional model as well as global model showed  
367 significantly different percentile distribution in all regions. Overall, both the medium  
368 and mean value of  $N_{rd}$  wet deposition were underestimated apparently in NC, SE and  
369 SW+TP, while similarly in NE and NW. The underestimation in NC was largely due  
370 to the under prediction in summer time not only in urban sites (Figure 3e) but also in  
371 rural sites (Figure 3f). Unfortunately, we cannot obtain the convincing temporal  
372 variation in SE and SW since the scarcely monthly data in these two regions (only one  
373 or two sites in each region). In NE, most of the models predicted similar temporal  
374 variations of  $N_{rd}$  wet deposition, especially the high depositions in summer time.

## 375 **3.2 Map of wet deposition among participant models**

### 376 **3.2.1 Wet deposition of oxidized N**

377 Figure 5 showed the map distribution of the yearly  $N_{ox}$  wet deposition simulated by  
378 each participant model, the ENM results and the observed results over China. Most  
379 models performed the similar spatial pattern with high level of deposition in central to  
380 eastern China and low level in western China. However, the threshold value in the  
381 Hotspot areas (from light yellow color to orange and red colors) varied significantly  
382 among the models and the average is much higher than the  $N_r$  deposition threshold  
383 value of  $10 \text{ kg N ha}^{-1}$  to the temperate ecosystems suggested by Bleeker et al.(2011).  
384 For example, M1, M5 and M11 simulated very high wet deposition of  $N_{ox}$  (almost  
385 reach at  $20 \text{ kg N ha}^{-1}$ ) in the middle Yangze River and Yangze River Delta (YRD),  
386 basin of Sichuan Province, south of NC and Liaoning Province located in NE. In



387 contrast, M2 and M14 failed to perform the relative hotspot  $N_{\text{wox}}$  in such areas, and  
388 M4, M6, M12 and M13 showed the obscure hotspot with small value of  $10 \text{ kg N ha}^{-1}$ .  
389 The significant differences do not only exist between different models but also in the  
390 same model CMAQ, i.e., M1, M2, M4, M5 and M6. Since most models were driven  
391 by the meteoroidal field and standard emission input except M13 (Geos-Chem) and  
392 M14 (RAMS-CMAQ), the differences in simulated  $N_{\text{ox}}$  wet deposition should come  
393 from the CTMs themselves, such as the diffusion and convection process, the  
394 oxidation and chemical transformation as well as the wet scavenging and deposition  
395 processes. The comparison of the long lifetime specie CO (Kong et al., 2019) and  
396 weak chemical activity specie BC (Chen et al., 2019b) revealed that the model  
397 uncertainties are less than other species, i.e.,  $\text{O}_3$  (Li et al., 2019) and  $\text{NO}_3^-$  (Chen et al.,  
398 2019b) which are strong chemical activity and short lifetime in the atmosphere. These  
399 results indicated that the chemical reaction process rather than the diffusion and  
400 convection process is one of the most important factors affecting the model  
401 uncertainties in MICS-Asia III.

### 402 3.2.2 Wet deposition of reduced N

403 Figure 6 showed the map distribution of the reduced N ( $N_{\text{rd}}$ ) wet deposition over  
404 China. All of the models performed similar spatial pattern with high values in central  
405 and eastern China but low level of deposition in NW and northwestern of NE.  
406 Compared with the  $N_{\text{ox}}$ , little differences of the simulated  $N_{\text{rd}}$  wet deposition were  
407 found among 9 models except M11, which predicted significant lower values.  $N_{\text{ox}}$  wet  
408 deposition of five agricultural dominant provinces including Shandong, Henan, Hubei,  
409 Hunan and Anhui is higher than the threshold value of  $10 \text{ kg N ha}^{-1}$  according to the  
410 simulated results by most models. Unfortunately, little observations in these areas  
411 made it harder to validate their truthfulness. Evidence showed the high level of  $N_{\text{rd}}$   
412 wet deposition over the threshold based on the observations in Hebei, YRD and Pearl  
413 River delta (PRD). Almost all of the models were under predicted in these areas. Liu  
414 et al. (2013) reported the important contribution of  $N_{\text{rd}}$  to the total N deposition in  
415 China based on the long-term national scale of observed nitrogen deposition data. In  
416 the agricultural predominant areas, the ammonia emission is the main contribution to  
417 the  $N_{\text{rd}}$  deposition (Liu et al., 2011 AE review; Kang et al., 2016). Thus, although the  
418 rarely observation cannot support the simulated high level of  $N_{\text{rd}}$  wet deposition in  
419 agricultural predominant regions, i.e., Shandong, Henan, Hubei, Hunan and Anhui,  
420 where the simulated  $N_{\text{rd}}$  wet depositions are higher than  $10 \text{ kg N ha}^{-1}$ , it may be more  
421 convincing that the  $N_{\text{rd}}$  wet deposition is higher than the threshold value according to  
422 the confirmed underestimation both in agricultural areas (i.e., Hebei) and in  
423 non-agricultural areas (i.e., YRD, PRD).

## 424 3.3 Comparisons among participant models for reactive N depositions

### 425 3.3.1 Coefficient of variations for N depositions in MICS-Asia III

426 Besides the wet deposition of oxidized and reduced N, dry deposition was also an  
427 important process for the total deposition part in China (Liu et al., 2013; Pan et al.,  
428 2012). Coefficient of Variation (hereinafter, CV), defined as the standard deviation  
429 divided by mean value of all selected model results, with large value denoting lower  
430 consistency among the models, is applied for model comparison of simulated reactive



431 N depositions both for dry and wet deposition process in MICS-Asia III. Figure 7  
432 shows the distribution of CV for each type of simulated reactive N depositions. Since  
433 the low level of mean values of deposition are more likely to associate with higher CV,  
434 the gridded CV was only calculated in the area with the simulated depositions higher  
435 than  $0.5 \text{ kg N ha}^{-1}$  (hereafter, analyzed value) in this study. As it is shown in Figure 7,  
436 the spatial distribution of CV only covered Eastern China, Southern China and  
437 Northeast China, which indicated that the quarterly and yearly fluxes of reactive N  
438 deposition in these regions was higher than the analyzed value. For annual case, the  
439 CV value of  $N_{\text{rd}}$  was lower compared with  $N_{\text{ox}}$  both for dry and wet depositions. This  
440 means the multi-model simulations were more consistent in  $N_{\text{rd}}$  depositions than in  
441  $N_{\text{ox}}$  depositions. More specifically, the  $N_{\text{rd}}$  in wet deposition has lowest CV values  
442 followed by  $N_{\text{rd}}$  in dry deposition and then the  $N_{\text{ox}}$  in wet and dry deposition, which  
443 suggested the simulated wet deposition of  $N_{\text{rd}}$  had less uncertainties than the other  
444 types of reactive N depositions.

445 More complicated patterns were shown in seasonal variations of each type of  
446 deposition. The simulated  $N_{\text{ox}}$  for dry deposition in Figure 7 (a) showed larger  
447 uncertainties in southern China (south of  $30^\circ \text{N}$ , with the  $\text{CV} > 0.4$ ) than that in  
448 northern China (north of  $30^\circ \text{N}$ , with the  $\text{CV} < 0.3$ ) in all seasons except summer.  
449 Similar spatial and temporal patterns of the CV values were found in  $N_{\text{rd}}$  dry  
450 deposition. It is worth noting that the large CV values with the range of 0.4-0.6 were  
451 exhibited in Central China (i.e., Henan, Hebei and Shandong provinces) during  
452 summer and autumn in spite of the high flux of  $N_{\text{rd}}$  dry deposition in these regions  
453 (map distribution of  $N_{\text{ox}}$  and  $N_{\text{rd}}$  dry deposition simulated in 9 participant models was  
454 displayed in Figure S3 and Figure S4 of the supplementary documents). This  
455 delivered an important message that the uncertainties of the physical and chemical  
456 processes in the participant models, including gas-particle equilibrium (Ge et al.,  
457 2019), dry deposition parameter scheme (Zhang et al., 2003), transportation as well as  
458 the chemical reaction with other acidifying substances (Liu et al., 2019), in the  
459 regions of high emission originated from agricultural activities in growing seasons  
460 may lead to significant deviation of simulated  $N_{\text{rd}}$  dry depositions.

461 For wet deposition of  $N_{\text{ox}}$ , large uncertainties were located in southern China in  
462 summer and autumn with the CV values higher than 0.6 compared with the CV values  
463 lower than 0.4 in other regions (Figure 7c). Anyway, this high value of CV was not  
464 found in the summer time of simulated  $N_{\text{rd}}$  wet deposition (Figure 7d). Due to the  
465 high portion of summer time flux to the total annual wet deposition, high CV value in  
466  $N_{\text{ox}}$  contributed to the most important part of the significantly larger annual CV value  
467 than that shown in the  $N_{\text{rd}}$  case. Due to the same rainfall input for the wet deposition  
468 in the framework of MICS-Asia III except model 13 and 14, the different CV values  
469 for  $N_{\text{rd}}$  and  $N_{\text{ox}}$  in same region (i.e., lower CV values of  $N_{\text{rd}}$  wet depositions in NC, SE  
470 and Central China) would attribute to their precursors concentration in the air mass as  
471 well as the different wet scavenging processes (Seinfeld and Pandis, 2006). This has  
472 been discussed in the following section.

### 473 3.3.2 Comparison of precursors in the air mass

474 As we all know, depositions both from dry and wet part of a certain substance were



475 originated from its precursor in the air mass. The uncertainties of the nitrogen related  
476 species in the air mass simulated during MICS-Asia III were therefore an important  
477 index for estimating the performance of deposition simulations. Figure 8 showed the  
478 distribution of CV for  $\text{NO}_x$ , particulate  $\text{NO}_3^-$ , gaseous  $\text{NH}_3$  and particulate  $\text{NH}_4^+$  in the  
479 air mass simulated by the 9 participant models during four seasons as well as the  
480 annual mean values. There were significant seasonal variations among the spatial  
481 patterns of the CV for each type of the N related air pollutants. It is interesting to note  
482 that not only the seasonal variations but also the spatial patterns of the simulated  
483 precursors' CV were reasonably consistent with those previously shown in the  
484 deposition part (Figure 7). For example, high CV values were found in the simulation  
485 of particulate  $\text{NO}_3^-$  in Southern China during summer, reaching to or even higher than  
486 0.8 in SE China (Figure 8b). The high CV values were also found in the summertime  
487 of  $\text{N}_{\text{ox}}$  wet deposition (Figure 7c). As the most important precursor of  $\text{N}_{\text{ox}}$  wet  
488 deposition (Pan et al., 2012), the correlated consistence between the precursor and the  
489 deposition is reasonable. This has also been proved in the distribution of CV values in  
490  $\text{NO}_x$  (Figure 8a) and  $\text{N}_{\text{ox}}$  dry depositions (Figure 7a) during autumn and winter.  
491 However, only uncertainties in precursors cannot explain everything, for example, the  
492 high CV values of  $\text{N}_{\text{ox}}$  wet deposition in south China was corresponding to the low  
493 CV values of  $\text{NO}_3^-$  in autumn. Some other factors, such as the scavenging process  
494 might be responsible for the unknown-uncertainties. Xu et al. (2017;2019) first  
495 compared the below-cloud wet scavenging coefficients based on the different  
496 estimation methods and found the magnitude difference between each type of  
497 methods. Thus, more detailed comparison such as in-cloud and below-cloud wet  
498 scavenging coefficients in each participant model should be carried out in the next  
499 phase of MICS-Asia.

500 As the most important precursor of  $\text{N}_{\text{rd}}$  dry deposition, gaseous  $\text{NH}_3$  also showed  
501 large CV values in central China during summer time ( $> 0.6$ ). There were also  
502 significant high CV values in south of Yangtze River during autumn and winter period  
503 (0.7-0.8 in south of Yangtze River vs 0.3-0.5 in north of Yangtze River). The similar  
504 pattern but not significant uncertainty was found in the simulated  $\text{N}_{\text{rd}}$  dry deposition  
505 (0.3-0.4 vs 0.2-0.3 in Figure 7b). Different from the particulate  $\text{NO}_3^-$ , very low CV  
506 values were shown in particulate  $\text{NH}_4^+$  during summer leading to the less deviation of  
507 simulated  $\text{N}_{\text{rd}}$  wet deposition than the  $\text{N}_{\text{ox}}$ . Therefore, the performance of the  
508 precursors' simulation was highly correlated with their depositions, while other  
509 factors such as wet scavenging process might lead to the unknown uncertainties but  
510 this need to be verified in the future.

## 511 4 Discussion

### 512 4.1 Ensemble results of reactive N deposition and comparison with satellite

513 Wang et al. (2008) first presented the ENM depositions of acidify species over East  
514 Asia based on MICS-Asia II simulations and found that the ENM afford better skill in  
515 simulating wet depositions than each single model. In the phase III of MICS-Asia, the  
516 ENM value of wet depositions both for  $\text{N}_{\text{ox}}$  and  $\text{N}_{\text{rd}}$  has also been validated by  
517 observations and shown in Figure 5l and Figure 6l. The simulated  $\text{N}_{\text{ox}}$  wet deposition  
518 and VWA concentration in rainfall exhibited larger dispersion around 1:1 line with the



519 correlation coefficients  $R$  were 0.23 and 0.54 in 83 sites over China than that found in  
520  $N_{rd}$ , which is concentrated around 1:2 line with the correlation coefficients  $R$  were  
521 0.32 and 0.8. This implicated the ensemble-mean value of simulated  $N_{ox}$  wet  
522 deposition has large uncertainties, while  $N_{rd}$  wet deposition was under predicted by a  
523 factor of two in MICS-Asia III. Compared to each single model, the ensemble-mean  
524 showed higher  $R$  value than most of single models. However, due to lack of direct  
525 observation of dry deposition, the validation for dry and total deposition of reactive N  
526 cannot be achieved. Instead, the column densities from satellite and emissions spatial  
527 distribution were employed to address the reasonability of the ensemble-mean of four  
528 types of reactive N depositions simulated in nine models. As displayed in Figure 9,  
529 dry depositions of  $N_{ox}$  and  $N_{rd}$  were concentrated in NC, YRD and Henan province,  
530 which is correspondence to the distribution of their emissions and VCDs, respectively.  
531 Meanwhile, wet depositions of  $N_{ox}$  and  $N_{rd}$  were centered at central China such as  
532 Hubei and Hunan province as well as Chengyu regions. Especially, there were high  
533 wet depositions of  $N_{rd}$  in south west of Hubei province and north east of Chengdu city,  
534 where high values of emissions and the VCDs for  $NH_3$  were absent. These regions  
535 loading with high wet depositions were mainly due to the high volume of rainfall (for  
536 more details at Figure S5) and the long-range transport of acidic substances (Ge et al.,  
537 2011).

538 Another interesting phenomenon was the different allocation of high values  
539 between depositions and VCD for  $N_{ox}$  and  $N_{rd}$ . For example, low depositions were  
540 loading in East China with high value of VCD for  $N_{ox}$  as the left panel of Figure 9  
541 shown. While as it was displayed in the right panel of Figure 9, large depositions of  
542  $N_{rd}$  in East China were corresponding to low level of VCD on the contrary. The whole  
543 emissions of  $NO_x$  and  $NH_3$  were similar at  $8 \text{ kg N}\cdot\text{ha}^{-1}$  ( $8.3 \text{ kg N}\cdot\text{ha}^{-1}$  and  $8.7 \text{ kg}$   
544  $\text{N}\cdot\text{ha}^{-1}$  for  $NO_x$  and  $NH_3$ , respectively) in China statistically from MICS-Asia III  
545 emission inventory. This implicated the allocation of both  $NO_x$  and  $NH_3$  between the  
546 deposition to the surface ground and staying in the atmosphere were conserved to  
547 their emission into the air. This conservation data from different sources also  
548 implicated the reasonable simulation of depositions for  $N_{ox}$  and  $N_{rd}$  in MICS-Asia III.

#### 549 **4.2 Contributions to the total inorganic N depositions and their potential effects**

550 Total inorganic N deposition (TIN), which includes the reduced and oxidized forms of  
551 inorganic N deposition both from wet and dry processes, has been calculated for  
552 estimating its ecosystem effects in this study as they were measured in most cases  
553 before (Pan et al., 2012; Liu et al., 2013). Figure 10 and Figure 11 showed the pathway  
554 of each type of N deposition to the TIN from spatial distribution view and 6 regions  
555 statistical results, respectively. The ENM dry depositions of gaseous  $HNO_3$  and  $NH_3$   
556 were the two major contributors to the TIN, both of which took part in 18% of TIN  
557 over the whole country; while the wet deposition of  $NO_3^-$  and  $NH_4^+$  were another two  
558 main components with the percentage of 23% and 28% (Table 4), respectively.  
559 Consistent with that reported in the global assessment under HTAP (Vet et al., 2014)  
560 and in nationwide monitoring network (NNDMN) estimation (Xu et al., 2015), the  $N_{rd}$   
561 in China dominated the TIN deposition with the averaged percentage reached at 52%  
562 for the ensemble results, although slightly lower compared with 60% and 58% in the



563 two previous works. The overall contribution of wet and dry deposition to TIN was  
564 almost half by half, which is consistent with that reported in NNDMN by Xu et al.  
565 (Xu et al., 2015). Considering the total emission, the depositions in whole China took  
566 about 67%, 65% and 66% in the 2010 emission of  $\text{NH}_3$ ,  $\text{NO}_x$  and total N  
567 ( $\text{NH}_3\text{-N}+\text{NO}_x\text{-N}$ ), respectively. It is interesting to show that the relationship of the  
568 gridded averaged  $N_{\text{rd}}$  deposition as well as the  $N_{\text{ox}}$  deposition with their relevant  
569 emissions in six regions (shown in Figure 12 with the slope: 0.56,  $r^2$ :0.97 for  $N_{\text{rd}}$  and  
570 the slope: 0.47,  $r^2$ :0.88 for  $N_{\text{ox}}$ ) were consistent with that reported by Xu et al. (Xu et  
571 al., 2015) (slope: 0.51,  $r^2$ :0.89 for  $N_{\text{rd}}$  and slope: 0.48,  $r^2$ :0.81 for  $N_{\text{ox}}$ ). Even the  
572 increasing trend of the regions from lowest in TP to highest in NC was the same as the  
573 previously measurement study. This implicated the spatial distribution as well as the  
574 relationships of deposition and emission were comparable with that measured in the  
575 NNDMN. Pan et al. (2013) also compared the correlations of the observed depositions  
576 vs emissions and attributed the inconsistent distribution between them in NCP to the  
577 uncertainties of the emission. However, the patterns of depositions were also  
578 influenced by the regional transport besides the emissions. In this study, significant  
579 positive correlations of the simulated  $N_{\text{ox}}(N_{\text{rd}})$  depositions with the correspondingly  
580  $\text{NO}_x(\text{NH}_3)$  emission reflected the control role of the relative emission to the spatial  
581 distribution of the depositions. Although most regions were located below 1:1 line of  
582 deposition to emission (Figure 12), few regions, such as TP and NE, were close to or  
583 above 1:1 line implied the impacts of transport on deposition among the regions.

584 For regions, the area-averaged deposition of TIN was highest as  $29.2 \text{ kg N}\cdot\text{ha}^{-1}$  and  
585  $27 \text{ kg N}\cdot\text{ha}^{-1}$  in NC and SE, followed by  $15 \text{ kg N}\cdot\text{ha}^{-1}$  and  $10.1 \text{ kg N}\cdot\text{ha}^{-1}$  in SW and  
586 NE, respectively. The TIN in NW and TP were lowest as  $3.1$  and  $2.7 \text{ kg N}\cdot\text{ha}^{-1}$ . In top  
587 brand of two highest regions NC and SE, the deposition of TIN was similar but the  
588 pathways to them were different. The  $N_{\text{rd}}$  deposition (53%) and the dry deposition  
589 (54%) contributed more than half portion of TIN in NC, while the  $N_{\text{ox}}$  deposition  
590 (55%) dominated the TIN in SE. Considering the lower ratio of  $\text{NO}_x/\text{NH}_3$  emission in  
591 SE (21.4/21.6, 0.99) than NC (30.4/24.4, 1.25), higher contribution of  $N_{\text{ox}}$  to TIN in  
592 SE indicated more oxidant ratio of the precursors than NC. For more oxidant N  
593 species, i.e.,  $\text{HNO}_3$  and  $\text{NO}_3^-$ , both dry and wet depositions were higher in SE than  
594 that shown in NC (5.8 vs. 4.9 for dry deposition of gaseous  $\text{HNO}_3$  and 6.9 vs. 6.3 for  
595 wet deposition of particulate  $\text{NO}_3^-$ ). While for less oxidant N and the reduced N, all  
596 type of depositions, such as dry deposition of gaseous  $\text{NO}_x$ , gaseous  $\text{NH}_3$  as well as  
597 the particulate  $\text{NH}_4^+$ , were less in SE than NC, except the wet deposition of particulate  
598  $\text{NH}_4^+$ , which would due to the much higher volume of rainfall in SE (Figure S5).  
599 Overall, the oxidant N made the emitted  $\text{NO}_x$  more easily to be scavenged in SE with  
600 the ratio of  $N_{\text{ox-deposition}}/\text{NO}_x\text{-emission}$  reaching at 70%, while the reduced N is  
601 more likely to be scavenged from its emission with the ratio as 64% in NC. The total  
602 ratio of TIN/emission in NC and SE were 53% and 63%, respectively. Compared to  
603 the Critical Load (Duan et al., 2001;Zhao et al., 2009;Liu et al., 2011), which is a  
604 judgement of the deposited N effects to the ecosystem, the two regions were almost  
605 reaching and even exceeding to the CL value (Table 4), indicating serious ecological  
606 impacts of the N deposition in NC and SE and should be paid more attention to the



607 controlling of the N related species, especially the  $N_{rd}$  in NC and  $N_{ox}$  in SE.

608 In the less developed economic and social area of SW, Due to the high emission of  
609  $NH_3$ , 60% of the TIN was dominated by  $N_{rd}$  deposition. The ratio of  $NO_x/NH_3$   
610 emission reached 0.49 as the more  $NH_3$  emitted from agricultural activity than the  
611  $NO_x$  from the fossil fuel consuming. The ratio of wet deposition/TIN was 55%, which  
612 was lower than the HTAP comparison during 2000 (60-70%) (Vet et al., 2014) but  
613 higher than the results of NNDMN (45%)(Xu et al., 2015). Although the undeveloped  
614 society, the TIN deposition was almost reaching at the CL value according to Zhao et  
615 al. (Zhao et al., 2009). Besides the high emission of  $NH_3$ , high ratio of  
616  $N_{ox}$ -deposition/ $NO_x$ -emission reaching at 94% reflecting the import of  $N_{ox}$  from high  
617 emitted area, such as SE and NC, should be attracted our attention in this region.  
618 Although the N deposition in TP was not reaching at CL value, which was the lowest  
619 in all regions of China with the value of  $2.7 \text{ kg N}\cdot\text{ha}^{-1}$ , the N ecological impacts  
620 cannot be neglected since the sensitive ecosystem (Shen et al., 2019) as well as the  
621 important climatically influence to whole China. Considering the high ratio of  
622 TIN/emission, which were larger than 1 with 3 for TIN, 2.71 for  $N_{rd}$  and 4 for  $N_{ox}$ , the  
623 import from outside was responsible to the N deposition in TP.

## 624 **5 Conclusion**

625 Reactive N depositions over China simulated in the frame work of MICS-Asia III  
626 have been compared within each participant models. Wet depositions were also  
627 validated by the multi-source of observations, i.e., recorded data from EANET, CAS,  
628 NNDMN and EPA of Guangdong and Liaoning province. Most models show the  
629 consistent spatial and temporal variation of both  $N_{ox}$  and  $N_{rd}$  wet depositions in China  
630 with the NME around at 50%, which is lower than the value of 70% based on EANET  
631 observation over Asia. Coefficient of Variation (CV) was applied for model  
632 comparison of dry deposition as well as the related precursor's concentration in the air  
633 mass. Consistence of both spatial and temporal variation of CV in deposition and the  
634 concentration in air mass indicated that performance of the precursors' simulation was  
635 highly correlated with their depositions.

636 Large deposition of ensemble simulation of  $N_{rd}$  deposition in eastern China was  
637 corresponding to low level of VCD from satellite measurement, while the case of  $N_{ox}$   
638 was just on the contrary. The total emission of  $NO_x$  and  $NH_3$  was similar at  $8 \text{ kg}$   
639  $N\cdot\text{ha}^{-1}$  in China. This indicated the allocation of both  $NO_x$  and  $NH_3$  between the  
640 deposition to the surface ground and staying in the atmosphere were conserved to  
641 their emission into the air, which also implicated the reasonable simulation of  
642 depositions for  $N_{ox}$  and  $N_{rd}$  in MICS-Asia III.

643 Wet deposition of nitrate and ammonium as well as the dry deposition of Gaseous  
644  $NH_3$  and  $HNO_3$  were the important pathway to TIN deposition with the percentage as  
645 18%, 18%, 23% and 28% for ensemble results, respectively. The gridded averaged  $N_{rd}$   
646 in China dominated the TIN deposition with the averaged percentage reached at 52%,  
647 which was slightly lower than the reported 60% and 58% in HTAP and NNDMN  
648 measurements. The contribution of wet and dry deposition to TIN was almost half by  
649 half and consistent with that reported in NNDMN. Even the ratio of TIN/emission  
650 was also similar with the NNDMN, indicating that the spatial distribution as well as



651 the relationships of deposition and emission were comparable with that measured in  
652 the NNDMN.

653 For different regions of China, the simulated  $N_{ox}$  wet deposition was overestimated  
654 in NE but underestimated in SE and SW, while large uncertainties were shown in NC.  
655 Two models simulated 30-50% higher of  $N_{ox}$  wet deposition, and four models were  
656 20~40% lower compared with observations in NC. The large divergences do not only  
657 exist between different models but also in the same CMAQ model, i.e., M1-M6. For  
658 the simulation of  $N_{rd}$  wet deposition, all the models were underpredicted in all regions,  
659 with the largest underestimation in NC and SE. Different from  $N_{ox}$ , almost similar  
660 behavior prediction of the less oxidative species such as the  $N_{rd}$  wet deposition has  
661 been found in CMAQ models, indicating the chemical reaction process is the one of  
662 the most importance factors affecting the model uncertainties in MICS-Asia III.  
663 Compared to CL value, the reactive N deposition in NC, SE and SW reached or  
664 exceeded the reported CL value and indicated serious ecological impacts. The control  
665 of  $N_{rd}$  in NC and SW and  $N_{ox}$  in SE would be effective to mitigate the TIN deposition  
666 in these regions. For the lowest reactive N deposition in TP, however, the N ecological  
667 impacts cannot be neglected since the sensitive ecosystem as well as the important  
668 climatically influence to whole China, especially considering the high ratio of  
669 TIN/emission, which was mainly caused by the import from outside. The joint  
670 prevention and control of air pollution in China should be carefully considered and  
671 implemented in the future.

672

### 673 **Acknowledgment**

674 We appreciate the Guangdong and Liaoning EPA for providing the observation data of  
675 Guangdong and Liaoning province. This work is supported by the National Natural  
676 Science Foundation of China (Grant No 41571130024, 41575123, 91744206,  
677 41330422) and the National Key Research and Development Plan  
678 (20017YFC0210100).





679 **Reference:**

- 680 Aikawa, M., and Hiraki, T.: Washout/rainout contribution in wet deposition estimated  
681 by 0.5 mm precipitation sampling/analysis, *Atmos Environ*, 43, 4935-4939, 2009.
- 682 Aikawa, M., Kajino, M., Hiraki, T., and Mukai, H.: The contribution of site to  
683 washout and rainout: Precipitation chemistry based on sample analysis from  
684 0.5 mm precipitation increments and numerical simulation, *Atmos Environ*, 95,  
685 165-174, <http://dx.doi.org/10.1016/j.atmosenv.2014.06.015>, 2014.
- 686 Bey, I., Jacob, D. J., Yantosca, R. M., Logan, J. A., Field, B. D., Fiore, A. M., Li, Q.  
687 B., Liu, H. Y., Mickley, L. J., and Schultz, M. G.: Global Modeling of  
688 Tropospheric Chemistry with Assimilated Meteorology: Model Description and  
689 Evaluation, *J.geophys.res*, 106, 23073–23095, 2001.
- 690 Bleeker, A., Hicks, W. K., Dentener, F., Galloway, J., and Erisman, J. W.: N deposition  
691 as a threat to the World’s protected areas under the Convention on  
692 Biological Diversity, *Environ Pollut*, 159, 2280-2288, 2011.
- 693 Byun, D., and Schere, K. L.: Review of the governing equations, computational  
694 algorithms, and other components of the models-3 Community Multiscale Air  
695 Quality (CMAQ) modeling system, *Appl. Mech. Rev.*, 59, 51–77,  
696 <https://doi.org/10.1115/1.2128636>, 2006.
- 697 Carlton, A. G., Bhave, P. V., Napelenok, S. L., Edney, E. O., Sarwar, G., Pinder, R. W.,  
698 Pouliot, G. A., and Houyoux, M.: 5 Model representation of secondary organic  
699 aerosol in CMAQv4.7, *Environ. Sci. Technol.*, 44(22), 8553–8560,  
700 <https://doi.org/10.1021/es100636q>, 2010.
- 701 Carmichael, G. R., Calori, G., Hayami, H., Uno, I., Cho, S. Y., Engardt, M., Kim, S.  
702 B., Ichikawa, Y., Ikeda, Y., Woo, J. H., Ueda, H., and Amann, M.: The  
703 MICS-Asia study: model intercomparison of long-range transport and sulfur  
704 deposition in East Asia, *Atmos Environ*, 36, 175-199, 2002.
- 705 Carmichael, G. R., Sakurai, T., Streets, D., Hozumi, Y., Ueda, H., Park, S. U., Fung,  
706 C., Han, Z., Kajino, M., Engardt, M., Bennet, C., Hayami, H., Sartelet, K.,  
707 Holloway, T., Wang, Z., Kannari, A., Fu, J., Matsuda, K., Thongbooncho, N., and  
708 Amann, M.: MICS-Asia II: The model intercomparison study for Asia Phase II  
709 methodology and overview of findings, *Atmos Environ*, 42, 3468-3490, 2008.
- 710 Carter, W. L.: Implementation of the SAPRC-99 chemical mechanism into the  
711 Models-3 framework, Report to the United States Environmental Protection  
712 Agency, available at: <http://www.engr.ucr.edu/~carter/pubs/s99mod3.pdf>, 2000,  
713 last access: 20 March 2019.
- 714 Chen, C., Park, T., Wang, X., Piao, S., Xu, B., Chaturvedi, R. K., Fuchs, R., Brovkin,  
715 V., Ciais, P., Fensholt, R., Tømmervik, H., Bala, G., Zhu, Z., Nemani, R. R., and  
716 Myneni, R. B.: China and India lead in greening of the world through land-use  
717 management, *Nature Sustainability*, 2, 122-129, [10.1038/s41893-019-0220-7](https://doi.org/10.1038/s41893-019-0220-7),  
718 2019a.
- 719 Chen, L., Gao, Y., Zhang, M., Fu, J. S., Zhu, J., Liao, H., Li, J., Huang, K., Ge, B.,  
720 Wang, X., Lam, Y. F., Lin, C. Y., Itahashi, S., Nagashima, T., Kajino, M., Yamaji,  
721 K., Wang, Z., and Kurokawa, J.: MICS-Asia III: multi-model comparison and  
722 evaluation of aerosol over East Asia, *Atmos. Chem. Phys.*, 19, 11911-11937,



- 723 10.5194/acp-19-11911-2019, 2019b.
- 724 Clark, C. M., and Tilman, D.: Loss of plant species after chronic low-level nitrogen  
725 deposition to prairie grasslands, *Nature*, 451, 712-715, 2008.
- 726 Clark, H., and Kremer, J. N.: Estimating direct and episodic atmospheric nitrogen  
727 deposition to a coastal waterbody, *Mar Environ Res*, 59, 349-366, 2005.
- 728 Colella, P., and Woodward, P. R.: The piecewise parabolic method (PPM) for gas  
729 dynamical simulations, *J. Comp. Phys.*, 54, 174–201, 1984.
- 730 Dise, N. B., and Wright, R. F.: Nitrogen leaching from European forests in relation to  
731 nitrogen deposition, *Forest Ecology & Management*, 71, 153-161, 1995.
- 732 Duan, L., Xie, S. D., Zhou, Z. P., Ye, X. M., and Hao, J. M.: Calculation and mapping  
733 of critical loads for S, N and acidity in China, *Water Air Soil Poll*, 130,  
734 1199-1204, 2001.
- 735 EANET: Technical Manual for Wet Deposition Monitoring in East Asia,  
736 <http://www.eanet.asia/product/manual/techwet.pdf>, 2010.
- 737 Erisman, J. W., Sutton, M. A., Galloway, J., Klimont, Z., and Winiwarter, W.: How a  
738 century of ammonia synthesis changed the world, *Nat Geosci*, 1, 636-639, 2008.
- 739 Fenn, M. E., Poth, M. A., Aber, J. D., Baron, J. S., Bormann, B. T., Johnson, D. W.,  
740 Lemly, A. D., McNulty, S. G., Ryan, D. F., and Stottlemyer, R.: NITROGEN  
741 EXCESS IN NORTH AMERICAN ECOSYSTEMS: PREDISPOSING  
742 FACTORS, ECOSYSTEM RESPONSES, AND MANAGEMENT  
743 STRATEGIES, *Ecol Appl*, 8, 706-733, 1998.
- 744 Fountoukis, C., and Nenes, A.: ISORROPIA II: A computationally efficient aerosol  
745 thermodynamic equilibrium model for K<sup>+</sup>, Ca<sup>2+</sup>, Mg<sup>2+</sup>, NH<sub>4</sub><sup>+</sup>, Na<sup>+</sup>, SO<sub>4</sub><sup>2-</sup>,  
746 NO<sub>3</sub><sup>-</sup>, Cl<sup>-</sup>, H<sub>2</sub>O aerosols, *Atmos. Chem. Phys.*, 7, 4639–4659, 2007.
- 747 Galloway, J. N., Dentener, F. J., Capone, D. G., Boyer, E. W., Howarth, R. W.,  
748 Seitzinger, S. P., Asner, G. P., Cleveland, C. C., Green, P. A., Holland, E. A., Karl,  
749 D. M., Michaels, A. F., Porter, J. H., Townsend, A. R., and Vorosmarty, C. J.:  
750 Nitrogen cycles: past, present, and future, *Biogeochemistry*, 70, 153-226, 2004.
- 751 Galloway, J. N., Townsend, A. R., Erisman, J. W., Bekunda, M., Cai, Z. C., Freney, J.  
752 R., Martinelli, L. A., Seitzinger, S. P., and Sutton, M. A.: Transformation of the  
753 nitrogen cycle: Recent trends, questions, and potential solutions, *Science*, 320,  
754 889-892, 2008.
- 755 Ge, B., Xu, X., Ma, Z., Pan, X., Wang, Z., Lin, W., Ouyang, B., Xu, D., Lee, J., Zheng,  
756 M., Ji, D., Sun, Y., Dong, H., Squires, F. A., Fu, P., and Wang, Z.: Role of  
757 Ammonia on the Feedback Between AWC and Inorganic Aerosol Formation  
758 During Heavy Pollution in the North China Plain, *Earth Space Sci*, 6, 1675-1693,  
759 10.1029/2019ea000799, 2019.
- 760 Ge, B. Z., Wang, Z. F., Xu, X. B., Tang, J., He, Y. J., Uno, I., and Ohara, T.: Impact of  
761 the East Asian summer monsoon on long-term variations in the acidity of summer  
762 precipitation in Central China, *Atmos Chem Phys*, 11, 1671-1684, DOI  
763 10.5194/acp-11-1671-2011, 2011.
- 764 Guenther, A., Karl, T., Harley, P., Wiedinmyer, C., Palmer, P. I., and Geron, C.:  
765 Estimates of global terrestrial isoprene emissions using MEGAN (Model of  
766 Emissions of Gases and Aerosols from Nature), *Atmos Chem Phys*, 6, 3181-3210,



- 2006.
- 768 Han, Z., Sakurai, T., Ueda, H., Carmichael, G. R., Streets, D., Hayami, H., Wang, Z.,  
769 Holloway, T., Engardt, M., Hozumi, Y., Park, S. U., Kajino, M., Sartelet, K., Fung,  
770 C., Bennet, C., Thongboonchoo, N., Tang, Y., Chang, A., Matsuda, K., and  
771 Amann, M.: MICS-Asia II: Model intercomparison and evaluation of ozone and  
772 relevant species, *Atmos Environ*, 42, 3491-3509, 2008.
- 773 Hayami, H., Sakurai, T., Han, Z., Ueda, H., Carmichael, G. R., Streets, D., Holloway,  
774 T., Wang, Z., Thongboonchoo, N., Engardt, M., Bennet, C., Fung, C., Chang, A.,  
775 Park, S. U., Kajino, M., Sartelet, K., Matsuda, K., and Amann, M.: MICS-Asia II:  
776 Model intercomparison and evaluation of particulate sulfate, nitrate and  
777 ammonium, *Atmos Environ*, 42, 3510-3527, 2008.
- 778 Holloway, T., Sakurai, T., Han, Z., Ehlers, S., Spak, S. N., Horowitz, L. W.,  
779 Carmichael, G. R., Streets, D. G., Hozumi, Y., Ueda, H., Park, S. U., Fung, C.,  
780 Kajino, M., Thongboonchoo, N., Engardt, M., Bennet, C., Hayami, H., Sartelet,  
781 K., Wang, Z., Matsuda, K., and Amann, M.: MICS-Asia II: Impact of global  
782 emissions on regional air quality in Asia, *Atmos Environ*, 42, 3543-3561, 2008.
- 783 Holtgrieve, G. W., Schindler, D. E., Hobbs, W. O., Leavitt, P. R., Ward, E. J., Bunting,  
784 L., Chen, G. J., Finney, B. P., Gregory-Eaves, I., Holmgren, S., Lisac, M. J., Lisi,  
785 P. J., Nydick, K., Rogers, L. A., Saros, J. E., Selbie, D. T., Shapley, M. D., Walsh,  
786 P. B., and Wolfe, A. P.: A Coherent Signature of Anthropogenic Nitrogen  
787 Deposition to Remote Watersheds of the Northern Hemisphere, *Science*, 334,  
788 1545-1548, 2011.
- 789 Holtslag, A. A. M., and Boville, B.: Local versus nonlocal boundary layer diffusion in  
790 a global climate model, *J. Clim.*, 6, 1825-1842, 1993.
- 791 Itahashi, S., Yumimoto, K., Uno, I., Hayami, H., Fujita, S. I., Pan, Y., and Wang, Y.: A  
792 15-year record (2001-2015) of the ratio of nitrate to non-sea-salt sulfate in  
793 precipitation over East Asia, *Atmos. Chem. Phys.*, 18, 2835-2852,  
794 10.5194/acp-18-2835-2018, 2018.
- 795 Itahashi, S., Ge, B., Sato, K., Fu, J. S., Wang, X., Yamaji, K., Nagashima, T., Li, J.,  
796 Kajino, M., Liao, H., Zhang, M., Wang, Z., Li, M., Kurokawa, J., Carmichael, G.  
797 R., and Wang, Z.: MICS-Asia III: Overview of model inter-comparison and  
798 evaluation of acid deposition over Asia, *Atmos. Chem. Phys. Discuss.*, 2019, 1-53,  
799 10.5194/acp-2019-624, 2019.
- 800 Janjic, Z.: The step-mountain eta coordinate model: Further developments of the  
801 convection, viscous sublayer, and turbulence closure schemes, *Mon. Weather*  
802 *Rev.*, 122, 927-945, 1994.
- 803 Janssens, I. A., Dieleman, W., Luyssaert, S., Subke, J. A., Reichstein, M., Ceulemans,  
804 R., Ciais, P., Dolman, A. J., Grace, J., Matteucci, G., Papale, D., Piao, S. L.,  
805 Schulze, E. D., Tang, J., and Law, B. E.: Reduction of forest soil respiration in  
806 response to nitrogen deposition, *Nat Geosci*, 3, 315-322, 2010.
- 807 Kajino, M., Ueda, H., Sato, K., and Sakurai, T.: Spatial distribution of the  
808 source-receptor relationship of sulfur in Northeast Asia, *Atmos Chem Phys*, 11,  
809 6475-6491, 2011.
- 810 Kajino, M., Sato, K., Inomata, Y., and Ueda, H.: Source-receptor relationships of



- 811 nitrate in Northeast Asia and influence of sea salt on the long-range transport of  
812 nitrate, *Atmos Environ*, 79, 67-78,  
813 <http://dx.doi.org/10.1016/j.atmosenv.2013.06.024>, 2013.
- 814 Kajino, M., Deushi, M., Sekiyama, T. T., Oshima, N., Yumimoto, K., Tanaka, T. Y.,  
815 Ching, J., Hashimoto, A., Yamamoto, T., Ikegami, M., Kamada, A., Miyashita, M.,  
816 Inomata, Y., Shima, S., Ueda, H., Maki, T., and Mikami, M.: NHM-Chem, the  
817 Japan Meteorological Agency's regional meteorology – chemistry model (v1.0):  
818 model description and aerosol representations, *Geosci. Model Dev. Discuss.*,  
819 <https://doi.org/10.5194/gmd-2018-128>, 2018.
- 820 Kajino, M., Deushi, M., Sekiyama, T. T., Oshima, N., Yumimoto, K., Tanaka, T. Y.,  
821 Ching, J., Hashimoto, A., Yamamoto, T., Ikegami, M., Kamada, A., Miyashita, M.,  
822 Inomata, Y., Shima, S., Takami, A., Shimizu, A., Hatakeyama, S., Sadanaga, Y.,  
823 Irie, H., Adachi, K., Zaizen, Y., Igarashi, Y., Ueda, H., Maki, T., and Mikami, M.,  
824 NHM-Chem, the Japan Meteorological Agency's regional meteorology –  
825 chemistry model: model evaluations toward the consistent predictions of the  
826 chemical, physical, and optical properties of aerosols, *J. Meteor. Soc. Japan*,  
827 97(2), 337-374, <http://dx.doi.org/10.2151/jmsj.2019-020>, 2019.
- 828 Kong, L., Tang, X., Zhu, J., Wang, Z., Fu, J. S., Wang, X., Itahashi, S., Yamaji, K.,  
829 Nagashima, T., Lee, H. J., Kim, C. H., Lin, C. Y., Chen, L., Zhang, M., Tao, Z., Li,  
830 J., Kajino, M., Liao, H., Sudo, K., Wang, Y., Pan, Y., Tang, G., Li, M., Wu, Q., Ge,  
831 B., and Carmichael, G. R.: Evaluation and uncertainty investigation of the NO<sub>2</sub>,  
832 CO and NH<sub>3</sub> modeling over China under the framework of MICS-Asia III,  
833 *Atmos. Chem. Phys. Discuss.*, 2019, 1-33, 10.5194/acp-2018-1158, 2019.
- 834 Li, J., Nagashima, T., Kong, L., Ge, B., Yamaji, K., Fu, J. S., Wang, X., Fan, Q.,  
835 Itahashi, S., Lee, H. J., Kim, C. H., Lin, C. Y., Zhang, M., Tao, Z., Kajino, M.,  
836 Liao, H., Li, M., Woo, J. H., Kurokawa, J., Wang, Z., Wu, Q., Akimoto, H.,  
837 Carmichael, G. R., and Wang, Z.: Model evaluation and intercomparison of  
838 surface-level ozone and relevant species in East Asia in the context of MICS-Asia  
839 Phase III – Part 1: Overview, *Atmos. Chem. Phys.*, 19, 12993-13015,  
840 10.5194/acp-19-12993-2019, 2019a.
- 841 Li, M., Zhang, Q., Kurokawa, J. I., Woo, J. H., He, K., Lu, Z., Ohara, T., Song, Y.,  
842 Streets, D. G., Carmichael, G. R., Cheng, Y., Hong, C., Huo, H., Jiang, X., Kang,  
843 S., Liu, F., Su, H., and Zheng, B.: MIX: a mosaic Asian anthropogenic emission  
844 inventory under the international collaboration framework of the MICS-Asia and  
845 HTAP, *Atmos. Chem. Phys.*, 17, 935-963, 10.5194/acp-17-935-2017, 2017.
- 846 Li, R., Cui, L., Zhao, Y., Zhang, Z., Sun, T., Li, J., Zhou, W., Meng, Y., Huang, K.,  
847 and Fu, H.: Wet deposition of inorganic ions in 320 cities across China:  
848 spatio-temporal variation, source apportionment, and dominant factors, *Atmos.*  
849 *Chem. Phys.*, 19, 11043-11070, 10.5194/acp-19-11043-2019, 2019b.
- 850 Li, Y., Schichtel, B. A., Walker, J. T., Schwede, D. B., Chen, X., Lehmann, C. M.,  
851 Puchalski, M. A., Gay, D. A., and Jr, C. J.: Increasing importance of deposition of  
852 reduced nitrogen in the United States, *Proc Natl Acad Sci U S A*, 113, 5874-5879,  
853 2016.
- 854 Lin, M., Oki, T., Bengtsson, M., Kanae, S., Holloway, T., and Streets, D. G.:



- 855 Long-range transport of acidifying substances in east Asia - Part II -  
856 Source-receptor relationships, *Atmos Environ*, 42, 5956-5967, DOI  
857 10.1016/j.atmosenv.2008.03.039, 2008.
- 858 Liu, M., Huang, X., Song, Y., Tang, J., Cao, J., Zhang, X., Zhang, Q., Wang, S., Xu, T.,  
859 Kang, L., Cai, X., Zhang, H., Yang, F., Wang, H., Yu, J. Z., Lau, A. K. H., He, L.,  
860 Huang, X., Duan, L., Ding, A., Xue, L., Gao, J., Liu, B., and Zhu, T.: Ammonia  
861 emission control in China would mitigate haze pollution and nitrogen deposition,  
862 but worsen acid rain, *Proceedings of the National Academy of Sciences*, 116,  
863 7760, 10.1073/pnas.1814880116, 2019.
- 864 Liu, X. J., Duan, L., Mo, J. M., Du, E. Z., Shen, J. L., Lu, X. K., Zhang, Y., Zhou, X.  
865 B., He, C. N., and Zhang, F. S.: Nitrogen deposition and its ecological impact in  
866 China: An overview, *Environ Pollut*, 159, 2251-2264, 2011.
- 867 Liu, X. J., Zhang, Y., Han, W. X., Tang, A. H., Shen, J. L., Cui, Z. L., Vitousek, P.,  
868 Erisman, J. W., Goulding, K., Christie, P., Fangmeier, A., and Zhang, F. S.:  
869 Enhanced nitrogen deposition over China, *Nature*, 494, 459-462, 2013.
- 870 Liu, H., Jacob, D. J., Bey, I., and Yantosca, R. M.: Constraints from  $^{210}\text{Pb}$  and  $^7\text{Be}$  on  
871 wet deposition and transport in a global three-dimensional chemical, *J. Geophys.*  
872 *Res.*, 2001, 106(D11), 12109–12128, 2001.
- 873 Mann, G. W., Carslaw, K. S., Reddington, C. L., Pringle, K. J., and Henzing, J. S.:  
874 Intercomparison and evaluation of global aerosol microphysical properties among  
875 AeroCom models of a range of complexity, *Atmospheric Chemistry & Physics*,  
876 14, 4679-4713, 2014.
- 877 Nenes, A., Pandis, S.N., and Pilinis, C.: ISORROPIA: A new thermodynamic  
878 equilibrium model for multiphase multicomponent inorganic aerosols, *Aquat.*  
879 *Geoch.*, 4, 123–152, 1998.
- 880 Nicolas, G., and Galloway, J. N.: An Earth-system perspective of the global nitrogen  
881 cycle, *Nature*, 451, 293-296, 2008.
- 882 Pan, Y. P., Wang, Y. S., Tang, G. Q., and Wu, D.: Wet and dry deposition of  
883 atmospheric nitrogen at ten sites in Northern China, *Atmos Chem Phys*, 12,  
884 6515-6535, 2012.
- 885 Phoenix, G. K., Hicks, W. K., Cinderby, S., Kuylenstierna, J. C. I., Stock, W. D.,  
886 Dentener, F. J., Giller, K. E., Austin, A. T., Lefroy, R. D. B., Gimeno, B. S.,  
887 Ashmore, M. R., and Ineson, P.: Atmospheric nitrogen deposition in world  
888 biodiversity hotspots: the need for a greater global perspective in assessing N  
889 deposition impacts, *Global Change Biol*, 12, 470-476, 2006.
- 890 Pielke, R. A., Cotton, W. R., Walko, R. L., Tremback, C. J., Lyons, W. A., Grasso, L.  
891 D., Nicholls, M. E., Moran, M. D., Wesley, D. A., Lee, T. J., and Copeland, J. H.:  
892 A comprehensive meteorological modeling system—RAMS, *Meteorol Atmos*  
893 *Phys*, 49, 69-91, 10.1007/BF01025401, 1992.
- 894 Pleim, J. E., Xiu, A., Finkelstein, P. L., and Otte, T. L.: A coupled land-surface and dry  
895 deposition model and comparison to field measurements of surface heat, moisture,  
896 and ozone fluxes. *Water Air Soil Pollut. Focus*, 1(5), 243–252,  
897 <https://doi.org/10.1023/A:1013123725860>, 2001.
- 898 Pleim, J. E.: A combined local and nonlocal closure model for the atmospheric



- 899 boundary layer, Part I: Model description and testing, *J. Appl. Meteor. Climatol.*,  
900 46, 1383–1395, 2007a.
- 901 Pleim, J. E.: A combined local and nonlocal closure model for the atmospheric  
902 boundary layer. Part II: Application and evaluation in a mesoscale meteorological  
903 model, *J. Appl. Meteorol. Clim.*, 46, 1396–1409, 2007b.
- 904 Seinfeld, J. H., and Pandis, S. N.: *Atmospheric chemistry and physics: from air*  
905 *pollution to climate change*, Wiley, New York, 2006.
- 906 Shen, H., Dong, S., Li, S., Xiao, J., Han, Y., Yang, M., Zhang, J., Gao, X., Xu, Y., Li,  
907 Y., Zhi, Y., Liu, S., Dong, Q., Zhou, H., and Yeomans, J. C.: Effects of simulated  
908 N deposition on photosynthesis and productivity of key plants from different  
909 functional groups of alpine meadow on Qinghai-Tibetan plateau, *Environ Pollut.*,  
910 251, 731-737, <https://doi.org/10.1016/j.envpol.2019.05.045>, 2019.
- 911 Sudo, K., Takahashi, M., Kurokawa, J. I., and Akimoto, H.: CHASER: A global  
912 chemical model of the troposphere 1. Model description, *Journal of Geophysical*  
913 *Research*, 107, ACH-1-ACH 7-20, 2002.
- 914 Tang, J., Chen, H. B., Yu, X. L., Wang, S., Yao, P., Lv, B., Xu, X. B., and Ding, G.:  
915 Evaluation of results of station inter-comparison with blind samples in Acid Rain  
916 Monitoring Network in China(in Chinese), *Meteoro. Monthly*, 33, 75–83, 2007.
- 917 Tang, J., Xu, X., Ba, J., and Wang, S.: Trends of the precipitation acidity over China  
918 during 1992-2006, *Chinese Sci Bul*, 5, 1-9, 2010.
- 919 van der Werf, G. R., Randerson, J. T., Giglio, L., Collatz, G. J., Mu, M., Kasibhatla, P.  
920 S., Morton, D. C., DeFries, R. S., Jin, Y., and van Leeuwen, T. T.: Global fire  
921 emissions and the contribution of deforestation, savanna, forest, agricultural, and  
922 peat fires (1997–2009), *Atmos. Chem. Phys.*, 10, 11707-11735,  
923 10.5194/acp-10-11707-2010, 2010.
- 924 Vet, R., Artz, R. S., Carou, S., Shaw, M., Ro, C. U., Aas, W., Baker, A., Bowersox, V.  
925 C., Dentener, F., Galy-Lacaux, C., Hou, A., Pienaar, J. J., Gillett, R., Forti, M. C.,  
926 Gromov, S., Hara, H., Khodzher, T., Mahowald, N. M., Nickovic, S., Rao, P. S. P.,  
927 and Reid, N. W.: A global assessment of precipitation chemistry and deposition of  
928 sulfur, nitrogen, sea salt, base cations, organic acids, acidity and pH, and  
929 phosphorus, *Atmos Environ*, 93, 3-100, 2014.
- 930 Walcek, C. J., and Aleksic, N. M.: A simple but accurate mass conservative  
931 peak-preserving, mixing ratio bounded advection algorithm with fortran code,  
932 *Atmos. Environ.*, 32, 3863–3880, 1998.
- 933 Wang, Y., Yu, W., Pan, Y., and Wu, D.: Acid neutralization of precipitation in Northern  
934 China, *J Air Waste Manag Assoc*, 62, 204-211, 2012.
- 935 Wang, Y. X., McElroy, M. B., Jacob, D. J., and Yantosca, R. M.: A nested grid  
936 formulation for chemical transport model over Asia: Applications to CO, *J.*  
937 *Geophys. Res.*, 109, D22307, <https://doi.org/10.1029/2004JD005237>, 2004.
- 938 Wang, Z. F., Xie, F. Y., Sakurai, T., Ueda, H., Han, Z. W., Carmichael, G. R., Streets,  
939 D., Engardt, M., Holloway, T., Hayami, H., Kajino, M., Thongboonchoo, N.,  
940 Bennet, C., Park, S. U., Fung, C., Chang, A., Sartelet, K., and Amann, M.:  
941 MICS-Asia II: Model inter-comparison and evaluation of acid deposition, *Atmos*  
942 *Environ*, 42, 3528-3542, 2008.



- 943 Wesely, M. L.: Parameterization of surface resistance to gaseous dry deposition in  
944 regional numerical models, *Atmos. Environ.*, 16, 1293–1304, 1989.
- 945 Xu, D., Ge, B., Wang, Z., Sun, Y., Chen, Y., Ji, D., Yang, T., Ma, Z., Cheng, N., Hao,  
946 J., and Yao, X.: Below-cloud wet scavenging of soluble inorganic ions by rain in  
947 Beijing during the summer of 2014, *Environ Pollut*, 230, 963–973,  
948 <https://doi.org/10.1016/j.envpol.2017.07.033>, 2017.
- 949 Xu, D., Ge, B., Chen, X., Sun, Y., Cheng, N., Li, M., Pan, X., Ma, Z., Pan, Y., and  
950 Wang, Z.: Multimethod determination of the below-cloud wet scavenging  
951 coefficients of aerosols in Beijing, China, *Atmos. Chem. Phys. Discuss.*, 2019,  
952 1–26, 10.5194/acp-2019-680, 2019.
- 953 Xu, W., Luo, X. S., Pan, Y. P., Zhang, L., Tang, A. H., Shen, J. L., Zhang, Y., Li, K. H.,  
954 Wu, Q. H., Yang, D. W., Zhang, Y. Y., Xue, J., Li, W. Q., Li, Q. Q., Tang, L., Lu,  
955 S. H., Liang, T., Tong, Y. A., Liu, P., Zhang, Q., Xiong, Z. Q., Shi, X. J., Wu, L.  
956 H., Shi, W. Q., Tian, K., Zhong, X. H., Shi, K., Tang, Q. Y., Zhang, L. J., Huang, J.  
957 L., He, C. E., Kuang, F. H., Zhu, B., Liu, H., Jin, X., Xin, Y. J., Shi, X. K., Du, E.  
958 Z., Dore, A. J., Tang, S., Collett, J. L., Goulding, K., Sun, Y. X., Ren, J., Zhang, F.  
959 S., and Liu, X. J.: Quantifying atmospheric nitrogen deposition through a  
960 nationwide monitoring network across China, *Atmos Chem Phys*, 15,  
961 12345–12360, 2015.
- 962 Yamartino, R. J.: Nonnegative, conserved scalar transport using grid-cell-centered,  
963 spectrally constrained Blackman cubics for applications on a variable-thickness  
964 mesh, *Mon. Weather Rev.*, 121, 753–763, 1993.
- 965 Zaveri, R. A., and Peters, L. K.: A new lumped structure photochemical mechanism  
966 for large-scale applications, *J. Geophys. Res.*, 104, 30387–30415, 1999.
- 967 Zhang, L., Brook, J. R., and Vet, R.: A revised parameterization for gaseous dry  
968 deposition in air-quality models, *Atmos.chem.phys*, 3, 2067–2082, 2003.
- 969 Zhao, Y., Duan, L., Xing, J., Larssen, T., Nielsen, C. P., and Hao, J. M.: Soil  
970 Acidification in China: Is Controlling SO<sub>2</sub> Emissions Enough?, *Environ Sci  
971 Technol*, 43, 8021–8026, 2009.
- 972



973 **Tables**

974 Table 1. Mechanism and parameterization of deposition part of MICS-Asia III

No	M1	M2	M4	M5	M6	M11	M12	M13	M14
Model- (version) <sup>a</sup>	CMAQ v5.0.2	CMAQ v5.0.2	CMAQ v4.7.1	CMAQ v4.7.1	CMAQ v4.7.1	NAQPMS	NHM-Chem	GEOS-Chem	CMAQ v4.7.1
Advection-H <sup>b</sup>	Yamo	Yamo	PPM	PPM	Yamo	WA	WA	TPCORE	PPM
Advection-V <sup>b</sup>	PPM	PPM	PPM	PPM	Yamo	WA	WA	TPCORE	PPM
Diffusion-H <sup>b</sup>	multiscale	multiscale	multiscale	multiscale	multiscale	BD	multiscale	HB	multiscale
Diffusion-V <sup>b</sup>	ACM2	ACM2	ACM2	ACM2	ACM2	K-theory	MYJ	HB	ACM2
Gas-Chemistry <sup>c</sup>	SAPRC-99	SAPRC-99	SAPRC-99	SAPRC-99	SAPRC-99	CBMZ	SAPRC-99	Bey	SAPRC-99
Aerosol-chemistry <sup>d</sup>	AERO6	AERO6	AERO5	AERO5	AERO5	ISORROPIA (v1.7)	ISORROPIA (v2.1)	ISORROPIA (2.1)	ISORROPIA (v1.7)
Cloud & Aqueous <sup>e</sup>	ISORROPIA (v2.1)	ISORROPIA (v2.1)	ISORROPIA (v1.7)	ISORROPIA (v1.7)	ISORROPIA (v1.7)	Ge	WC	Jacob	ACM
Dry dep <sup>f</sup>	ACM-AE6	ACM-AE6	ACM-AE5	ACM-AE5	ACM-AE5	Wesely	Kajino	Wesely & Wang	M3DRY
Wet dep <sup>g</sup>	M3DRY	M3DRY	M3DRY	M3DRY	M3DRY	Ge	Kajino	Liu	Foley
Met	Foley	Foley	Foley	Foley	ACM	WRF	WRF	GEOS-5	RAMS
Emission <sup>h</sup>	WRF	WRF	WRF	WRF	WRF	standard	standard	standard	standard

975

976 <sup>a</sup>: References for the advection scheme are as follows: Yamo: Yamartino, 1993; PPM: Piecewise Parabolic Method (Colella and Woodward,  
 1984); WA: Walcek and Aleksic, 1998; TPCORE: Wang et al., 2004.

977 <sup>b</sup>: References for diffusion scheme are as follows: ACM2: Asymmetric Convective Model version 2 (Pleim, 2007a,b); BD: Byun and Dennis,  
 1995; HB: Holtlag and Boville, 1993; multiscale: Byun and Schere, 2006; MYJ: Janjic, 1994.

24





980 <sup>c</sup>: References for the gas phase chemistry are as follows: Bey: Bey et al., 2001; CBMZ: Zaveri and Peters, 1999; SAPRC-99: Carter, 2000.  
981 <sup>d</sup>: References for the aerosol chemistry are as follows: ISORROPIA version 2.1: Fountoukis and Nenes, 2007; version 1.7: Nenes et al., 1998.  
982 <sup>e</sup>: References for the Cloud & Aqueous are as follows: Ge: Ge et al., 2014; WC: Walcek, 1986 and Carlton, 2007; Jacob: Jacob, 2000;  
983 <sup>f</sup>: References for the dry deposition scheme are as follows: M3DRY: Pleim et al., 2001; Kajino: Kajino et al., 2018; Wang: Wang et al., 2004;  
984 Wesely: Wesely, 1989.  
985 <sup>g</sup>: References for the wet deposition scheme are as follows: Foley: Foley et al, 2010; Ge: Ge et al., 2014; Kajino: Kajino et al., 2018; Liu: Liu et  
986 al., 2001.  
987 <sup>h</sup>: “standard” indicates the basic emission inventories in Phase III.  
988  
989



Table 2. Statistical parameters of oxidized N deposition for urban, rural and whole China.

Urban (N=49)	OBS	M1	M2	M4	M5	M6	M11	M12	M13	M14
Oxidized N deposition (kg N ha <sup>-1</sup> )										
R	0.24	0.25	0.28	0.27	0.26	0.25	0.40	0.37	0.22	
NMB%	16.8%	-44.5%	-19.3%	38.5%	-15.8%	48.2%	-5.3%	-7.2%	-52.7%	
NME%	56.4%	60.4%	51.3%	64.0%	51.0%	67.1%	46.9%	44.2%	59.1%	
FAC2%	63.3%	32.7%	51.0%	57.1%	57.1%	59.2%	57.1%	61.2%	40.8%	
Mean	7.1	8.3	3.9	5.7	9.9	6.0	10.5	6.7	6.6	3.4
Oxidized N concentration in rainfall (mg N/L)										
R	0.60	0.57	0.60	0.62	0.59	0.49	0.61	0.52	0.50	
NMB%	26.8%	-37.9%	-11.3%	49.3%	-6.7%	75.9%	2.7%	19.3%	-31.3%	
NME%	57.6%	51.4%	46.0%	69.0%	47.5%	94.8%	47.4%	65.5%	60.0%	
FAC2%	59.2%	42.9%	59.2%	51.0%	59.2%	51.0%	61.2%	49.0%	34.7%	
Mean	0.9	1.1	0.5	0.8	1.3	0.8	1.5	0.9	1.0	0.6
Rural (N=34)										
Oxidized N deposition (kg N ha <sup>-1</sup> )										
R	0.09	0.05	0.09	0.14	0.09	0.28	0.26	0.23	0.30	
NMB%	55.4%	-27.8%	5.1%	86.9%	9.9%	102.5%	11.5%	13.6%	-37.6%	
NME%	83.7%	57.8%	59.9%	103.3%	60.5%	110.1%	54.4%	56.0%	50.3%	
FAC2%	55.9%	41.2%	50.0%	35.3%	47.1%	38.2%	55.9%	55.9%	50.0%	
Mean	5.4	8.5	3.9	5.7	6.0	11.0	6.1	6.2	3.4	
Oxidized N concentration in rainfall (mg N/L)										
R	0.43	0.41	0.44	0.46	0.44	0.48	0.47	0.35	0.43	
NMB%	20.5%	-43.0%	-17.1%	45.2%	-13.4%	63.2%	-9.4%	-0.2%	-43.2%	
NME%	65.4%	55.6%	54.2%	76.3%	53.8%	89.2%	53.8%	62.7%	53.3%	
FAC2%	44.1%	38.2%	41.2%	41.2%	44.1%	41.2%	47.1%	32.4%	41.2%	



Mean	0.9	1.0	0.5	0.7	1.2	0.7	1.4	0.8	0.9	0.5
All sites (N=83)										
Oxidized N deposition (kg N ha <sup>-1</sup> )										
R	0.2	0.21	0.17	0.21	0.21	0.19	0.24	0.37	0.33	0.23
NMB%	30.3%	-10.7%	-38.7%	-10.7%	55.4%	-6.8%	67.2%	0.6%	0.1%	-47.4%
NME%	66.0%	54.3%	59.5%	54.3%	77.8%	54.3%	82.2%	49.5%	48.3%	56.0%
FAC2%	60.2%	50.6%	36.1%	50.6%	48.2%	53.0%	50.6%	56.6%	59.0%	44.6%
Mean	6.4	8.4	3.9	5.7	10.0	6.0	10.7	6.5	6.4	3.4
Oxidized N concentration in rainfall (mg N/L)										
R	0.53	0.51	0.54	0.54	0.56	0.53	0.48	0.56	0.46	0.46
NMB%	24.2%	-40.0%	-13.7%	-13.7%	47.6%	-9.5%	70.7%	-2.3%	11.3%	-36.2%
NME%	60.8%	53.1%	49.4%	49.4%	72.0%	50.1%	92.5%	50.0%	64.4%	57.3%
FAC2%	53.0%	41.0%	51.8%	51.8%	47.0%	53.0%	47.0%	55.4%	42.2%	37.3%
Mean	0.9	1.1	0.5	0.7	1.3	0.8	1.5	0.8	1.0	0.5



993 Table 3. Same as Table 2 but for reduced N deposition.

Urban (N=49)	OBS	M1	M2	M4	M5	M6	M11	M12	M13	M14
Reduced N deposition (kg N ha <sup>-1</sup> )										
R	0.30	0.31	0.33	0.34	0.32	0.41	0.33	0.49	0.05	0.05
NMB%	-38.2%	-43.0%	-45.6%	-43.9%	-37.3%	-73.5%	-38.8%	-38.8%	-60.2%	-60.2%
NME%	50.7%	52.2%	52.9%	51.4%	49.8%	73.5%	50.0%	46.3%	64.1%	64.1%
FAC2%	53.1%	44.9%	42.9%	46.9%	51.0%	16.3%	51.0%	55.1%	34.7%	34.7%
Mean	10.9	6.2	5.9	6.1	6.8	2.9	6.7	6.7	4.3	4.3
Reduced N concentration in rainfall (mg N/L)										
R	0.83	0.83	0.84	0.84	0.83	0.77	0.86	0.75	0.56	0.56
NMB%	-38.0%	-42.6%	-42.2%	-40.6%	-36.1%	-73.8%	-41.1%	-22.1%	-48.8%	-48.8%
NME%	44.5%	47.5%	47.4%	46.0%	43.7%	73.8%	43.7%	46.0%	62.1%	62.1%
FAC2%	57.1%	51.0%	42.9%	51.0%	55.1%	10.2%	57.1%	44.9%	24.5%	24.5%
Mean	1.5	0.9	0.9	0.9	1.0	0.4	0.9	1.2	0.8	0.8
Rural (N=34)										
Reduced N deposition (kg N ha <sup>-1</sup> )										
R	0.29	0.29	0.28	0.30	0.32	0.27	0.28	0.52	0.44	0.44
NMB%	-14.4%	-22.0%	-21.1%	-18.3%	-13.6%	-62.5%	-23.2%	-19.0%	-46.2%	-46.2%
NME%	48.0%	47.7%	48.1%	46.5%	47.2%	68.5%	45.8%	40.8%	49.4%	49.4%
FAC2%	70.6%	55.9%	58.8%	61.8%	67.6%	23.5%	61.8%	73.5%	52.9%	52.9%
Mean	9.0	7.7	7.1	7.3	7.7	3.4	6.9	7.3	4.8	4.8
Reduced N concentration in rainfall (mg N/L)										
R	0.79	0.79	0.81	0.82	0.80	0.74	0.82	0.69	0.55	0.55
NMB%	-27.5%	-34.2%	-31.9%	-29.7%	-26.4%	-69.0%	-33.8%	-20.2%	-47.4%	-47.4%
NME%	37.7%	40.6%	39.0%	36.6%	37.1%	69.6%	37.9%	40.5%	56.9%	56.9%
FAC2%	52.9%	52.9%	52.9%	52.9%	55.9%	17.6%	52.9%	64.7%	44.1%	44.1%



Mean	1.3	1.0	0.9	0.9	0.9	1.0	0.4	0.9	1.1	0.7
	All sites (N=83)									
Reduced N deposition (kg N ha <sup>-1</sup> )										
R	0.26	0.27	0.26	0.27	0.28	0.30	0.29	0.48	0.20	0.20
NMB%	-29.6%	-35.3%	-36.7%	-34.5%	-28.6%	-69.5%	-33.1%	-31.6%	-55.1%	-55.1%
NME%	49.7%	50.6%	51.2%	49.6%	48.9%	71.7%	48.5%	44.3%	58.7%	58.7%
FAC2%	60.2%	49.4%	49.4%	53.0%	57.8%	19.3%	55.4%	62.7%	42.2%	42.2%
Mean	10.1	7.1	6.4	6.6	7.2	3.1	6.8	6.9	4.5	4.5
Reduced N concentration in rainfall (mg N/L)										
R	0.81	0.81	0.82	0.83	0.81	0.75	0.84	0.73	0.56	0.56
NMB%	-34.0%	-39.4%	-38.2%	-36.4%	-32.3%	-71.9%	-38.3%	-21.3%	-48.3%	-48.3%
NME%	41.9%	44.9%	44.2%	42.3%	41.2%	72.2%	41.5%	43.9%	60.1%	60.1%
FAC2%	55.4%	51.8%	47.0%	51.8%	55.4%	13.3%	55.4%	53.0%	32.5%	32.5%
Mean	1.4	0.9	0.9	0.9	1.0	0.4	0.9	1.1	0.7	0.7



995 Table 4. Types of depositions and its relevant contributions to TIN as well as the  
 996 emissions of reduced and oxidized N in different regions (Unit: kg N/ha/yr).

Regions		NC	NE	NW	SE	SW	TP	China
Types of deposit ion	gHNO3d	4.9	1.8	0.8	5.8	2.4	0.2	2.1
	gNH3d	6.7	1.8	0.5	3.7	3.0	0.5	2.0
	gNOxd	1.2	0.3	0.1	1.0	0.3	0.0	0.3
	pNH4d	1.9	0.5	0.2	1.5	0.8	0.1	0.6
	pNO3d	1.3	0.4	0.1	1.2	0.4	0.0	0.4
	pNH4w	7.0	2.6	0.8	7.0	5.2	1.3	3.2
	pNO3w	6.3	2.7	0.7	6.9	3.0	0.6	2.6
	N <sub>rd</sub>	15.6	4.9	1.6	12.2	9.0	1.9	5.9
	N <sub>ox</sub>	13.6	5.2	1.6	14.9	6.0	0.8	5.4
	Wet TIN	13.3	5.3	1.5	13.9	8.2	1.9	5.8
Dry TIN	16.0	4.8	1.7	13.2	6.9	0.8	5.5	
TIN	29.2	10.1	3.1	27.0	15.0	2.7	11.3	
N <sub>rd</sub> /TI N %	This study	53	49	52	45	60	70	52
	NNDMN							58
	HTAP							>60
Wet/TI N %	This study	46	52	48	51	55	70	51
	NNDMN	43	46	39	58	45	50	48
	HTAP	40~50	40~60	30~60	~60	60~70	60~70	
Emissi on	N <sub>rd</sub>	24.4	4.9	2.9	21.6	13.1	0.7	8.7
	N <sub>ox</sub>	30.4	5.6	3.1	21.4	6.4	0.2	8.3
	TIN	54.8	10.5	5.9	43.0	19.5	0.9	17.1
Dep/E mi %	N <sub>rd</sub>	64	100	55	56	69	271	67
	N <sub>ox</sub>	45	93	52	70	94	400	65
	TIN	53	96	53	63	77	300	66
Critical load	SSMB1	10~30	5~20	<5	10~20	>20	10~15	
	Empirical*	>200	<15	<15	50~200	50~200	20~50	
	SSMB2	>50	14~50	<14	20~50	10~30	~14	

997 1, Duan et al.,2, Zhao et al.,\* Liu et al.,,



998 **Figures and captions**

999 **Figure 1:** Locations of the measurement sites and the distribution of the ID.

1000 **Figure 2:** Percentile Box plot of oxidized N wet deposition simulated in each model  
1001 and compared with the observation as well as the rainfalls, with 99% and 1%  
1002 represented for the top and low points, 90% and 10% represented for the top and low  
1003 horizontal line, 75% and 25% represented for the upper and lower edge of the box and  
1004 asterisk and long horizontal line in the middle of the box represented for the medium  
1005 and mean value, respectively.

1006 **Figure 3:** Monthly variation of simulated wet deposition of oxidized N compared  
1007 with the observations in urban sites (a) and rural sites (b) of NC; urban sites (c) and  
1008 rural sites (d) of NE; as well as of reduced N in urban sites (e) and rural sites (f) of  
1009 NC; urban sites (g) and rural sites (h) of NE.

1010 **Figure 4:** Same as Figure 2 but for reduced N wet depositions.

1011 **Figure 5:** Distributions of the wet depositions of  $N_{ox}$  simulated by M1~M14 (a)~(i),  
1012 ENM of the multi-models (j) MICS-Asia III, observation from multi source  
1013 measurements (k) and the comparison between ENM and observations (l) ( $kgN \cdot ha^{-1}$ ).

1014 **Figure 6:** Same as Figure 5 but for  $N_{rd}$ .

1015 **Figure 7:** Spatial distribution of CV of (a)  $N_{ox}$  dry deposition, (b)  $N_{rd}$  dry deposition,  
1016 (c)  $N_{ox}$  wet deposition and (d)  $N_{rd}$  wet deposition in MICS-Asia III on the annual and  
1017 seasonal basis.

1018 **Figure 8:** Distribution of CV of  $NO_x$  (a),  $NO_3^-$  (b),  $NH_3$  (c) and  $NH_4^+$  (d) in the air  
1019 mass for seasonal and annual.

1020 **Figure 9:** ENM results for dry deposition (a) and wet deposition (b) of  $N_{ox}$ , VCD of  
1021  $NO_2$  from SCIAMACHY (c) and  $NO_x$  emission from MICS-Asia (d); ENM results for  
1022 dry deposition (e) and wet deposition (f) of  $N_{rd}$ , VCD of  $NH_3$  from IASI (g) and  $NH_3$   
1023 emission from MICS-Asia (h).

1024 **Figure 10:** ENM results of each process of N deposition flux (a) and the fraction in  
1025 TIN (b) in MICS-Asia III. The icons  $w_N$ ,  $w_A$ ,  $d_{NO_2}$ ,  $d_{NH_3}$ ,  $d_{HNO_3}$ ,  
1026  $d_{ammonium}$  and  $d_{nitrate}$  represented wet deposition of nitrate, wet deposition of  
1027 ammonium, dry deposition of  $NH_3$ , dry deposition of  $HNO_3$ , dry deposition of  
1028 ammonium and dry deposition of nitrate, respectively.

1029 **Figure 11:** Pathway of N species to TIN deposition in different regions from ENM  
1030 results (a), and TIN depositions by wet or dry deposited manner (b) in percentile Box  
1031 plot; with 90% and 10% represented for the top and low horizontal line, 75% and 25%  
1032 represented for the upper and lower edge of the box and asterisk in the middle of the

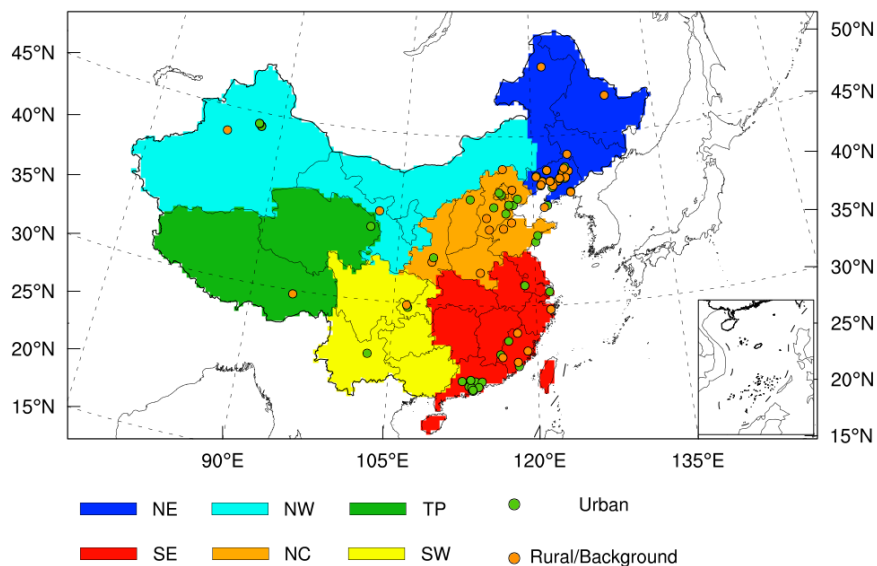


1033 box represented for the medium value, respectively.

1034 **Figure 12:** Relationship of  $N_{rd}$  deposition vs.  $NH_3$  emission (a) and relationship of  
1035  $N_{ox}$  deposition vs.  $NO_x$  emission (b) in each region of China.

1036

1037



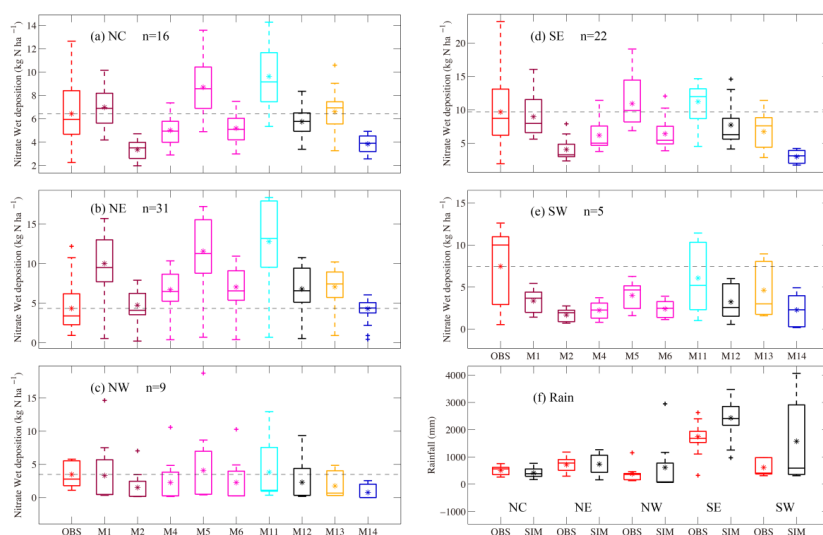
1038

1039 Figure 1: Locations of the measurement sites and the distribution of the ID



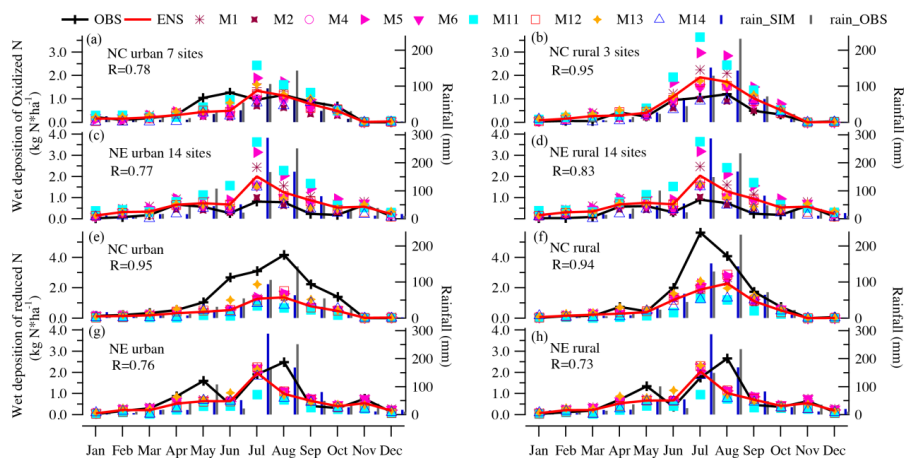


1040



1041

1042 Figure 2: Percentile Box plot of oxidized N wet deposition simulated in each model  
1043 and compared with the observation as well as the rainfalls, with 99% and 1%  
1044 represented for the top and low points, 90% and 10% represented for the top and low  
1045 horizontal line, 75% and 25% represented for the upper and lower edge of the box and  
1046 asterisk and long horizontal line in the middle of the box represented for the medium  
1047 and mean value, respectively

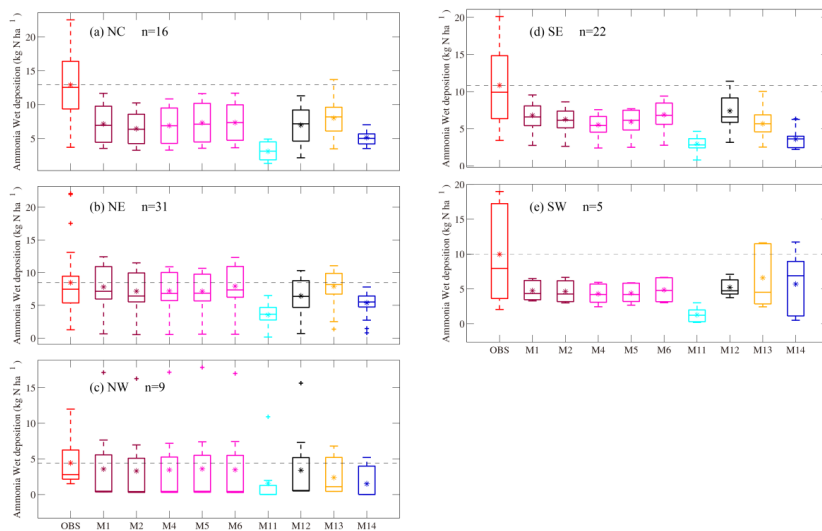


1048

1049 Figure 3: Monthly variation of simulated wet deposition of oxidized N compared with  
1050 the observations in urban sites (a) and rural sites (b) of NC; urban sites (c) and rural  
1051 sites (d) of NE; as well as of reduced N in urban sites (e) and rural sites (f) of NC;  
1052 urban sites (g) and rural sites (h) of NE



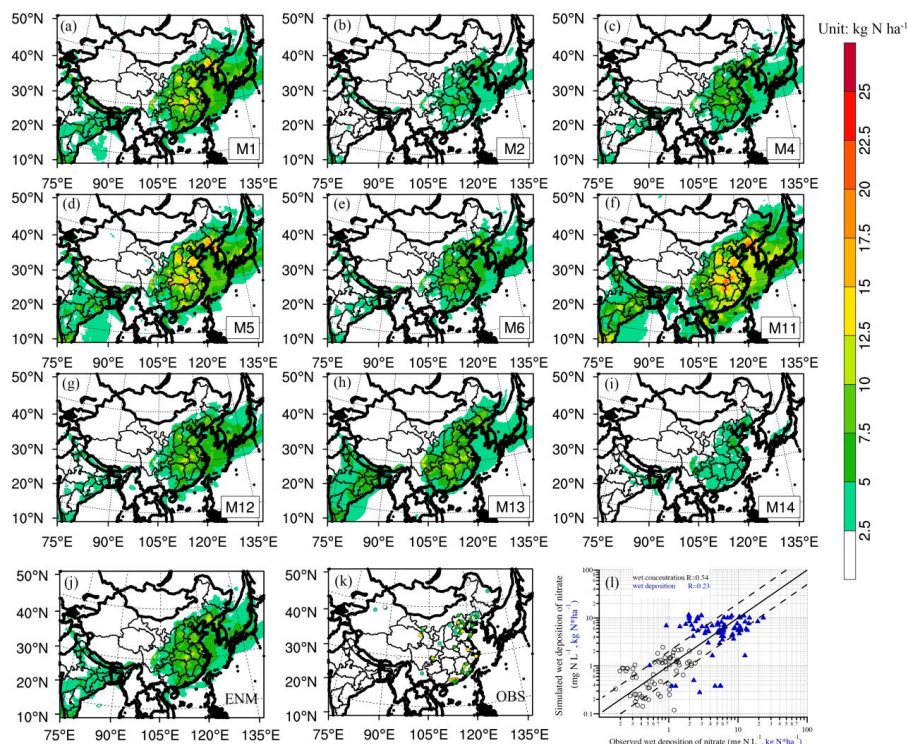
1053



1054

1055 Figure 4: Same as Figure 2 but for reduced N wet depositions

1056

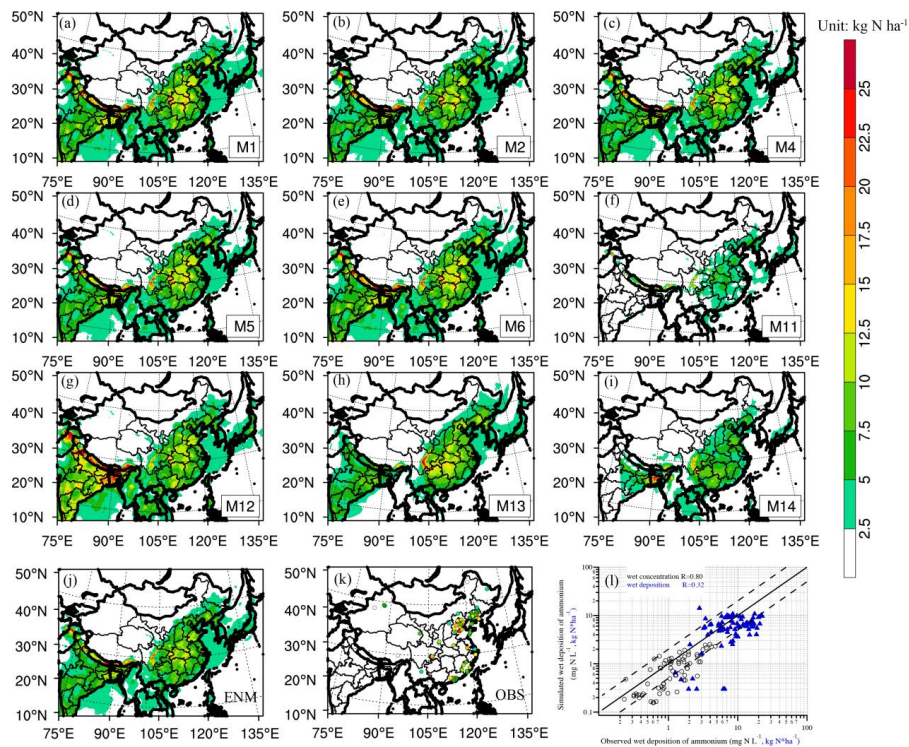


1057  
1058  
1059  
1060  
1061

Figure 5: Distributions of the wet depositions of  $\text{NO}_x$  simulated by M1~M14 (a)~(i), ENM of the multi-models (j) MICS-Asia III, observation from multi source measurements (k) and the comparison between ENM and observations (l) ( $\text{kgN}\cdot\text{ha}^{-1}$ )



1062

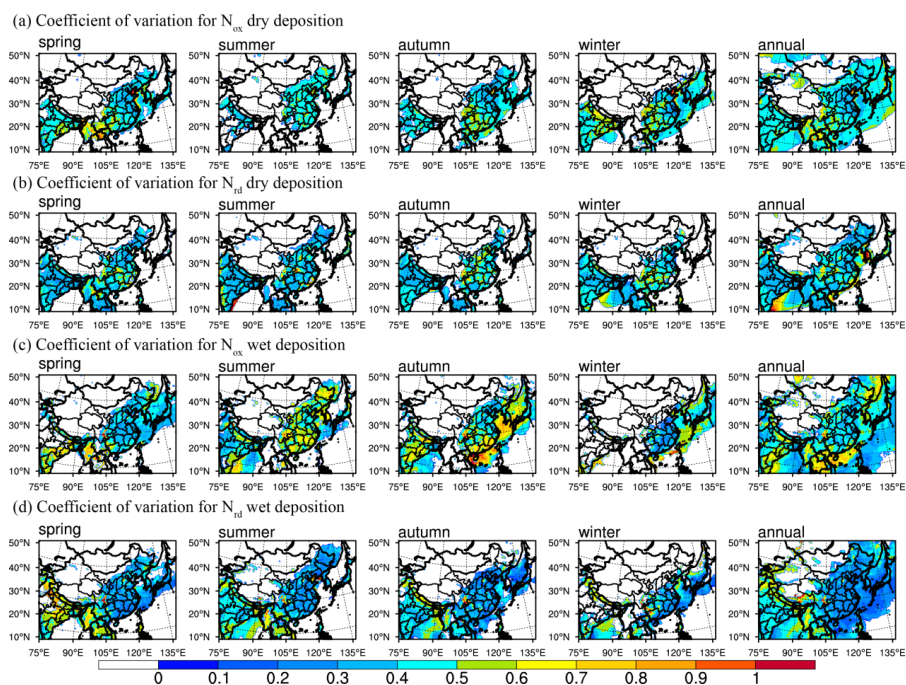


1063

1064 Figure 6: Same as Figure 5 but for  $N_{rd}$

1065

1066



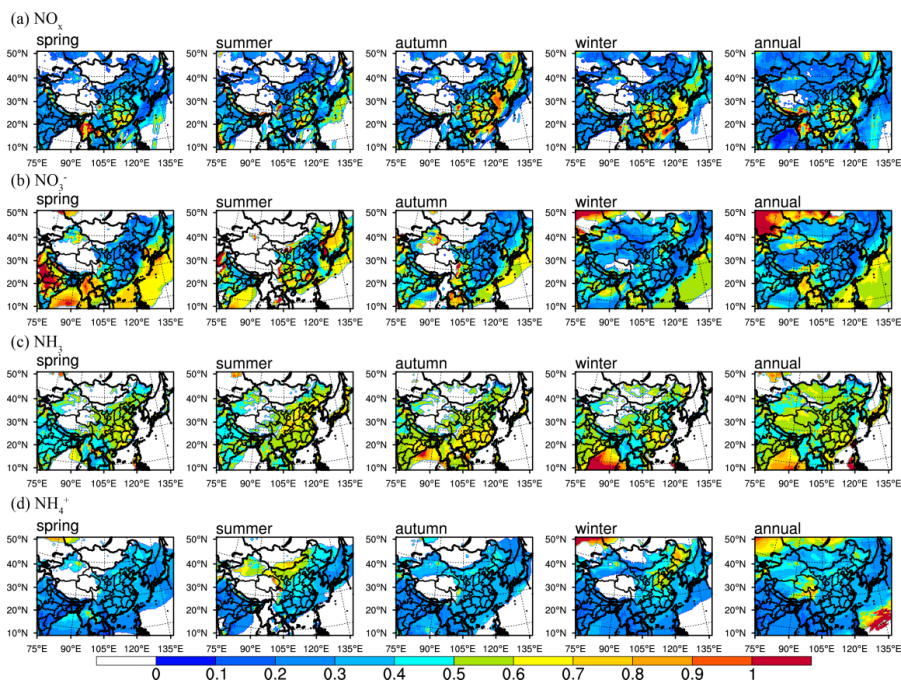
1067

1068 Figure 7: Spatial distribution of CV of (a)  $N_{ox}$  dry deposition, (b)  $N_{rd}$  dry deposition,  
1069 (c)  $N_{ox}$  wet deposition and (d)  $N_{rd}$  wet deposition in MICS-Asia III on the annual and  
1070 seasonal basis

1071



1072

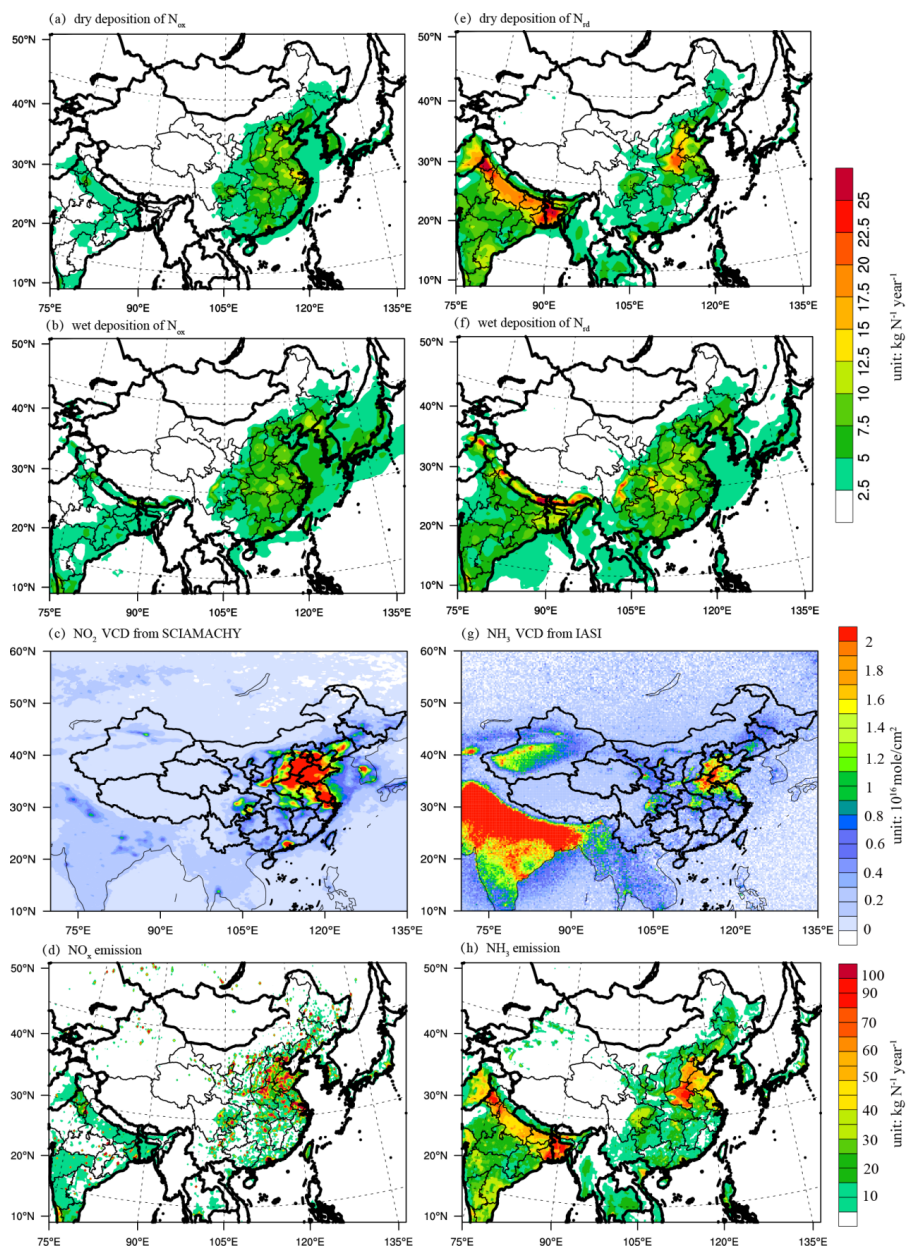


1073

1074 Figure 8: Distribution of CV of  $\text{NO}_x$  (a),  $\text{NO}_3^-$  (b),  $\text{NH}_3$  (c) and  $\text{NH}_4^+$  (d) in the air  
1075 mass for seasonal and annual

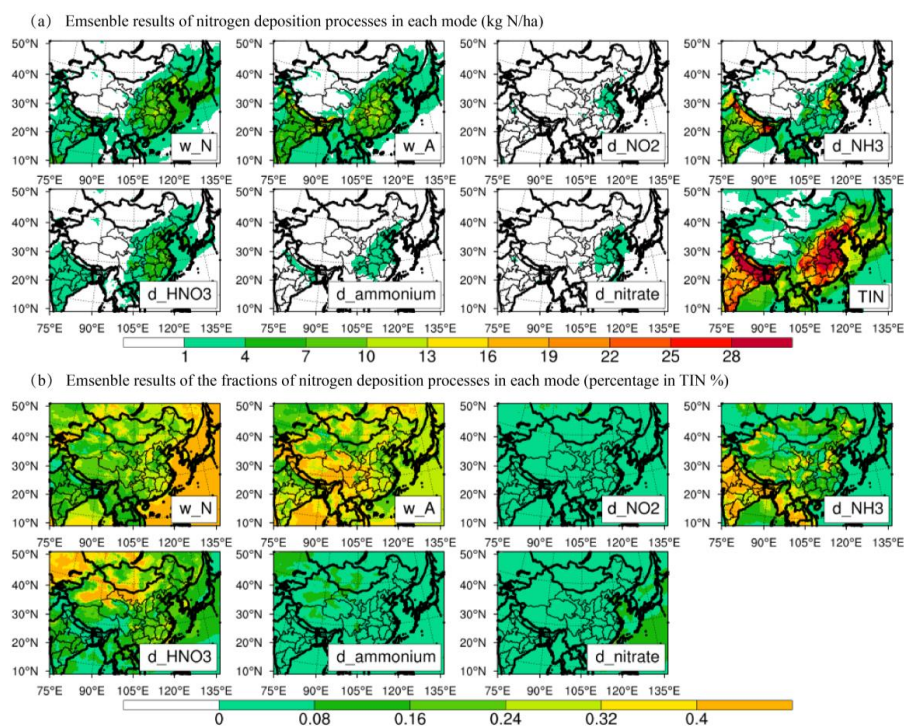
1076

1077



1078  
1079 Figure 9: ENM results for dry deposition (a) and wet deposition (b) of  $N_{ox}$ , VCD of  
1080  $NO_2$  from SCIAMACHY (c) and  $NO_x$  emission from MICS-Asia (d); ENM results for  
1081 dry deposition (e) and wet deposition (f) of  $N_{rd}$ , VCD of  $NH_3$  from IASI (g) and  $NH_3$   
1082 emission from MICS-Asia (h)





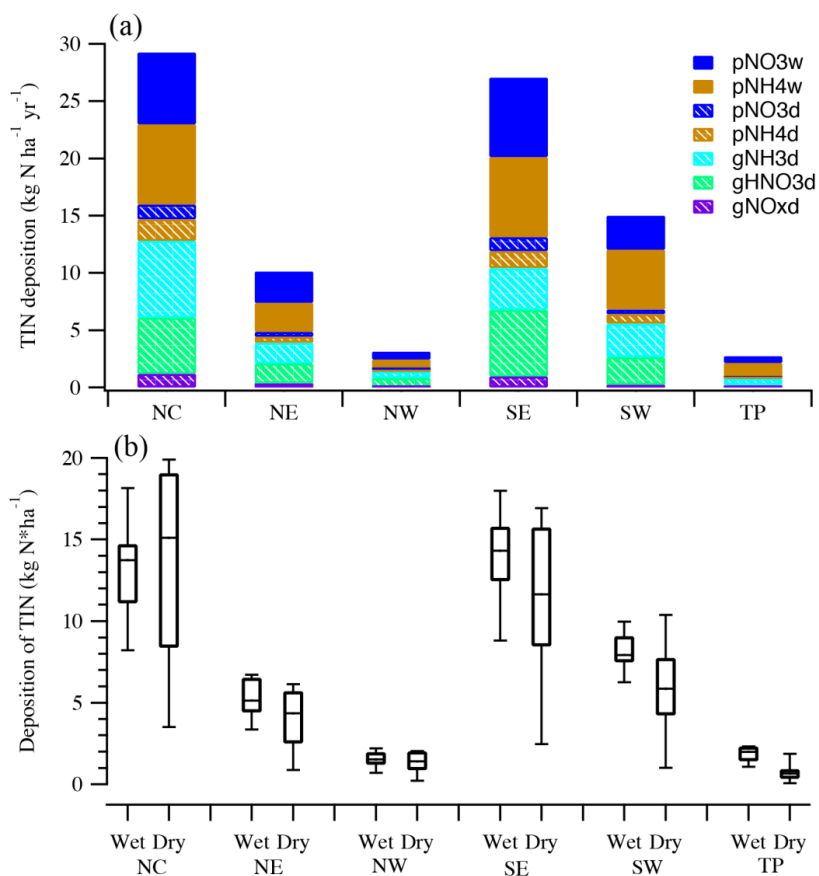
1083

1084 Figure 10: ENM results of each process of N deposition flux (a) and the fraction in  
1085 TIN (b) in MICS-Asia III. The icons  $w_N$ ,  $w_A$ ,  $d_{NO_2}$ ,  $d_{NH_3}$ ,  $d_{HNO_3}$ ,  
1086  $d_{ammonium}$  and  $d_{nitrate}$  represented wet deposition of nitrate, wet deposition of  
1087 ammonium, dry deposition of  $NH_3$ , dry deposition of  $HNO_3$ , dry deposition of  
1088 ammonium and dry deposition of nitrate, respectively.

1089



1090

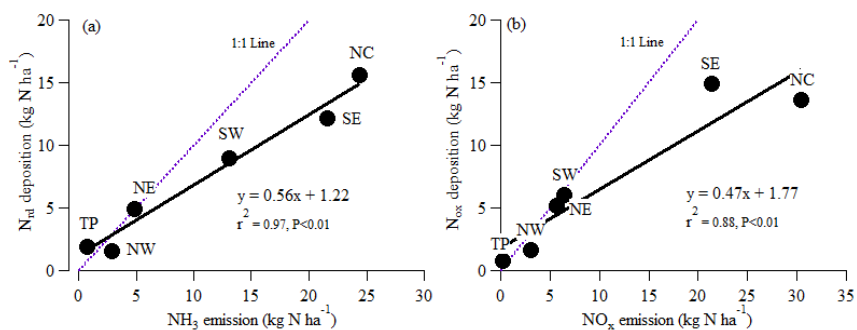


1091

1092 Figure 11: Pathway of N species to TIN deposition in different regions from ENM  
1093 results (a), and TIN depositions by wet or dry deposited manner (b) in percentile Box  
1094 plot; with 90% and 10% represented for the top and low horizontal line, 75% and 25%  
1095 represented for the upper and lower edge of the box and asterisk in the middle of the  
1096 box represented for the medium value, respectively



1097



1098

1099 Figure 12: Relationship of N<sub>rd</sub> deposition vs. NH<sub>3</sub> emission (a) and relationship of N<sub>ox</sub>  
1100 deposition vs. NO<sub>x</sub> emission (b) in each region of China

1101